SEDIMENTOLOGY the journal of the International Association of Sedimentologists

Sedimentology (2010) **57,** 1430–1462 doi: 10.1111/j.1365-3091.2010.01151.x

Middle and late Cenomanian oceanic anoxic events in shallow and deeper shelf environments of western Morocco

BRIAN GERTSCH*, THIERRY ADATTE†, GERTA KELLER*, ABDEL AZIZ A.M. TANTAWY‡, ZSOLT BERNER§, HAYDON P. MORT¶ and DOMINIK FLEITMANN**
**Department of Geosciences, Princeton University, Princeton, NJ 08544, USA (E-mail: bgertsch@princeton.edu)*
†Institut de Géologie et Paléontologie, Université de Lausanne, Anthropole, CH-1015 Lausanne, Switzerland
‡Department of Geology, Faculty of Science, South Valley University, Aswan 81528, Egypt
§Institute for Mineralogy & Geochemistry, University of Karlsruhe, 76128 Karlsruhe, Germany
¶Department of Earth Sciences – Geochemistry, Faculty of Geosciences, Utrecht University, PO Box 80.021, 3508 TA Utrecht, The Netherlands
***Institute of Geological Sciences, University of Bern, CH-3012 Bern, Switzerland*

Associate Editor – Tracy Frank

ABSTRACT

The response of shallow-water sequences to oceanic anoxic event 2 and mid-Cenomanian events 1a and 1b was investigated along the west African margin of Morocco north of Agadir (Azazoul) and correlated with the deep-water sequence of the Tarfaya Basin (Mohammed Beach) based on biostratigraphy, mineralogy, phosphorus and stable isotopes. In the deeper Mohammed Beach section results show double peaks in $\delta^{13}C_{org}$ for mid-Cenomanian events 1a and 1b (*Rotalipora reicheli* biozone, lower CC10a biozone), the characteristic oceanic anoxic event 2 $\delta^{13}C$ excursion (*Rotalipora cushmani* extinction, top of CC10a biozone) and laminated (anoxic) black shale. In the shallow environment north of Agadir, a fluctuating sea-level associated with dysoxic, brackish and mesotrophic conditions prevailed during the middle to late Cenomanian, as indicated by oyster biostromes, nannofossils, planktonic and benthonic foraminiferal assemblages. Anoxic conditions characteristic of oceanic anoxic event 2 (for example, laminated black shales) did not reach into shallow-water environments until the maximum transgression of the early Turonian. Climate conditions decoupled along the western margin of Morocco between mid-Cenomanian event 1b and the Cenomanian–Turonian boundary, as also observed in eastern Tethys. North of Agadir alternating humid and dry seasonal conditions prevailed, whereas in the Tarfaya Basin the climate was dry and seasonal. This climatic decoupling can be attributed to variations in the Intertropical Convergence Zone and in the intensity of the north-east trade winds in tropical areas.

Keywords Middle Cenomanian event, Morocco, oceanic anoxic event 2, palaeoclimate, shallow shelf environments.

INTRODUCTION

The middle to late Cretaceous is characterized by very warm climate and high sea-levels, which is attributed commonly to high concentrations of greenhouse gases related to increased tectonic activity (Larson, 1991; Larson & Erba, 1999). During this time, low-latitude basins of the western Tethys and North Atlantic intermittently experienced times of black shale deposition known as oceanic anoxic events (OAEs) (Jenkyns, 1980; Arthur *et al.*, 1988; Kerr, 1998; Leckie *et al.*,

2002). The main oceanic anoxic event, known as OAE2, is geographically the most extensive (Kerr, 1998) and spans the latest Cenomanian (*ca* 94 to 93·5 Ma) to early Turonian. Two smaller black shale depositional events occurred in the middle Cenomanian and are known as middle Cenomanian events (MCE) 1a and 1b (Rodriguez-Lazaro *et al.*, 1998; Coccioni & Galeotti, 2003; Jarvis *et al.*, 2006; Gale *et al.*, 2008).

The two MCEs have not been studied extensively. Their age is estimated at *ca* 95·8 Ma (Rodriguez-Lazaro *et al.*, 1998; Coccioni & Galeotti, 2003; Gale *et al.*, 2008). Sediments are characterized by relatively high total organic carbon (TOC) (<4%), two positive $\delta^{13}C$ excursions of about 2·2‰ and 2·5‰ (Jenkyns *et al.*, 1994; Paul *et al.*, 1994), minor faunal and floral turnovers (Paul *et al.*, 1994) and rapid sea-level fluctuations (Haq *et al.*, 1987; Paul *et al.*, 1994).

The well-studied late Cenomanian OAE2 was significantly more severe. A major transgression reached its maximum during the early Turonian (Haq *et al.*, 1987; Hallam, 1992) accompanied by very warm temperatures (Huber *et al.*, 1995, 2002; Clarke & Jenkyns, 1999; Norris *et al.*, 2002; Voigt *et al.*, 2004; Forster *et al.*, 2007). Marine biota experienced major faunal and floral turnovers (Erbacher *et al.*, 1996; Keller *et al.*, 2001, 2008; Leckie *et al.*, 2002; Erba & Tremolada, 2004; Keller & Pardo, 2004a), accompanied by a positive 2‰ carbon isotope excursion and black shale deposition (Hart & Leary, 1989; Uličný *et al.*, 1993; Paul *et al.*, 1999; Keller *et al.*, 2001, 2004; Tsikos *et al.*, 2004; Kuhnt *et al.*, 2005). Large igneous province eruptions were active in the Caribbean, Ontong Java and Madagascar during this period (Sinton *et al.*, 1998; Wignall, 2001; Courtillot & Renne, 2003; Snow *et al.*, 2005; Turgeon & Creaser, 2008) and are postulated as a major trigger of the late Cenomanian OAE2 (Kerr, 1998; Turgeon & Creaser, 2008).

During OAE2, organic-rich black shale deposition occurred in outer shelf and deep basin environments. Factors influencing black shale deposition include organic terrestrial influx and/or marine primary productivity, increased organic matter (OM) preservation and/or primary productivity, oxidation in the water column, rates of sedimentation, distance to the coast and water depth (Pedersen & Calvert, 1990; Arthur & Sageman, 1994; Canfield, 1994). The severity of oceanic anoxia in the water column depends largely on which of these factors was prevalent. Deeper basins near upwelling areas, such as the north-eastern Atlantic off Morocco (for example, the Tarfaya Basin), reveal very high sedimentation rates and organic contents (up to 8 cm per 10^3 years; Kuhnt *et al.*, 2005; Kolonic *et al.*, 2005). The Tarfaya Basin has been studied widely to evaluate variations in the intensity of anoxia, the magnitude and nature of the $\delta^{13}C$ excursion, the biotic effects on benthonic and planktonic foraminifera and the biostratigraphic record (Kuhnt *et al.*, 1997, 2005, 2009; Kolonic *et al.*, 2005; Mort *et al.*, 2007, 2008; Keller *et al.*, 2008).

Shallower middle shelf environments (100 to 200 m depth), such as the US Western Interior at Pueblo, Colorado (*ca* 100 m), reveal higher terrigenous influx and lower organic contents (Pratt *et al.*, 1993; Sageman *et al.*, 1998; Keller *et al.*, 2004). Pueblo, as well as the similarly shallow Eastbourne section in England (200 to 300 m), provide excellent biostratigraphic control and a wealth of information on water column anoxia (causes, variations in intensity and faunal consequences), the nature of the $\delta^{13}C$ excursion and patterns of sedimentation related to OAE2 conditions in middle shelf environments (Leckie *et al.*, 1998, 2002; Paul *et al.*, 1999; Gale *et al.*, 2000; Keller *et al.*, 2001; Keller & Pardo, 2004a; Caron *et al.*, 2006; Sageman *et al.*, 2006).

Black shales are rare in sections from inner ramp and coastal environments, either because they were not deposited or were not preserved (Van Buchem *et al.*, 2002; Luning *et al.*, 2004). The biostratigraphic record is generally poor due to low-diversity and long-ranging stress-resistant assemblages (Keller & Pardo, 2004a,b; Gertsch *et al.*, 2010). As a result, these environments have received little attention to date and, consequently, are poorly understood with regard to palaeoenvironmental conditions during OAEs (Schlanger *et al.*, 1987; Drzewiecky & Simo, 1997; Davey & Jenkyns, 1999; Voigt *et al.*, 2006; Parente *et al.*, 2007; Gertsch *et al.*, 2010). Largely unanswered questions concern the overall response of shallow shelf environments to oceanic anoxia. Did the low oxygen water mass reach into inner ramp and coastal environments? If so, what was the timing? What were the biotic effects? At what rate did OM accumulate? Is the absence of black shale a matter of dilution by terrigenous influx or preservation? Investigation of shallow neritic and coastal sections can provide some answers to these questions.

This study focuses on shallow neritic sections of western Morocco and deeper shelf sections of the Tarfaya Basin in order to evaluate and compare the middle and late Cenomanian anoxic events. It is hypothesized that OAE2 reached into

very shallow waters, but that the effects were mitigated by oxygen uptake in surface waters such that the water column never reached the oxygen depletion of deeper shelf or basin environments. In addition, the signal was lessened probably by high terrigenous influx and generally poor OM preservation. If this hypothesis is correct, then the sea water composition in shallow neritic environments should retain the $\delta^{13}C$ signal that is characteristic ocean-wide, even though other factors (for example, biotic effects and TOC) may vary.

The shallow-water coastal section at Azazoul north of Agadir, Morocco, and the deeper shelf/basin section at Mohammed Beach in the Tarfaya Basin of southern Morocco (Fig. 1A) were selected to test this hypothesis. Investigations concentrate on: (i) stable isotopes ($\delta^{13}C$) to evaluate the shallow-water response in relation to global oceanic productivity; (ii) mineralogy and sedimentology to evaluate the depositional environment and climate evolution; (iii) OM and phosphorus contents to glean information on primary productivity; (iv) faunal turnovers to evaluate the biotic response to anoxia and environmental stress; and (v) biostratigraphy and age control.

GEOLOGICAL SETTING AND LOCATION

The Azazoul section is exposed in two segments separated by a 5 to 10 m landslide along the coast about 20 km north of Agadir (Fig. 1A). The lower middle Cenomanian segment crops out along the Agadir to Essaouira Road, whereas the upper middle Cenomanian to Turonian segment crops out along the nearby beach.

Palaeogeographically, the Azazoul section is situated on the rim of the Agadir and Essaouira Basins, which belong to the northern part of the Tarfaya Basin. During the Cenomanian to early Turonian, a large marine seaway marks the Agadir Gulf between the Idrissides High and Anti-Atlas chain (Fig. 1B), which represents the arm of a failed rift of the North Atlantic rift system (Luning *et al.*, 2004). In the Agadir Gulf, sediments consist of organic-poor inner shelf deposits, including alternating marl-limestone layers and oyster-rich limestone beds. Deposition varied between inner to middle shelf environments without significant upwelling (Behrens *et al.*, 1978; Wiedmann *et al.*, 1978, 1982; Jati, 2007).

By contrast, the Mohammed Beach section (Fig. 1A) is located in the widely studied Tarfaya Basin to the south, which extends along the

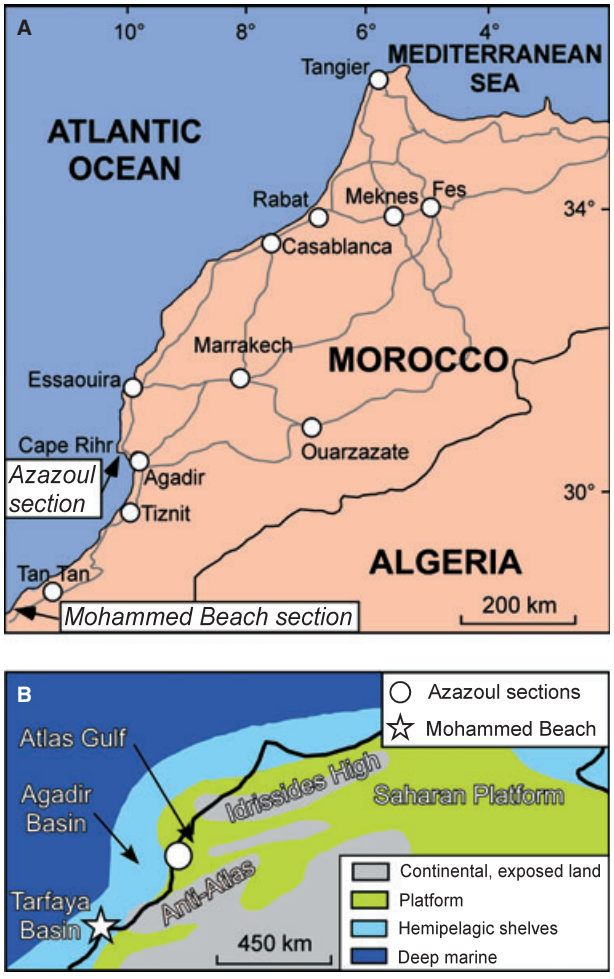

Fig. 1. (A) Geographical map of north-western Morocco and locations of Azazoul and Mohammed Beach sections (grey lines: roads). (B) Palaeogeographic map of north-west Africa during the Cenomanian with the position of Azazoul and Mohammed Beach sections (modified from Luning *et al.*, 2004).

southern coast of Morocco between 28°N and 24°N (Fig. 1A). Both MCE and OAE2 are present, although only the OAE2 has been studied thoroughly. During the late Cenomanian and early Turonian, OAE2 is characterized by thick units of organic-rich marls with high TOC (11% to 18%) and thin limestone layers (Kuhnt *et al.*, 1997; Kuypers *et al.*, 2002; Gustafsson *et al.*, 2003; Luning *et al.*, 2004; Kolonic *et al.*, 2005; Kuhnt *et al.*, 2005; Keller *et al.*, 2008; Mort *et al.*, 2008).

METHODS

Sections were examined in the field for lithological changes, burrows, macrofossils, hardgrounds and erosion surfaces, which were described, measured and photographed. A total of 257

samples were collected at an average interval of 25 cm for the Azazoul Beach outcrop and 104 samples for the road outcrop at intervals of about 10 cm. A further 120 samples were collected at Mohammed Beach. In the laboratory, samples were processed for foraminiferal analysis using standard methods (Keller *et al.*, 1995). Planktonic foraminifera were analysed in the >63 μm size fraction. Species identification follows that of Sliter (1968), Robaszynski & Caron (1979), Caron (1985) and Bolli *et al.* (1994).

Samples were processed for nannofossil analysis using methods described in Tantawy (2003) and Perch-Nielsen (1985). This study follows the standard cosmopolitan zonations of Sissingh (1977) and Perch-Nielsen (1985) and incorporates additional bioevents from Bralower (1988) and Burnett (1998).

Carbon and oxygen isotope analyses were carried out on powdered bulk rock samples at the stable isotope laboratories at the University of Karlsruhe, Germany, using an Optima ratio mass spectrometer (Micromass UK Limited, Manchester, UK) equipped with an online carbonate preparation line (Multi Carb; Micromass UK Limited) with separate vials for each sample, and at the University of Bern, Switzerland, using a Finnigan Delta V Advantage mass spectrometer equipped with an automated carbonate preparation (Gas-Bench II) (Thermo Fischer Scientific AG, Reinach, Switzerland). The results were calibrated to the Vienna Pee Dee Belemnite (V-PDB) scale with standard errors of 0·05‰ for $\delta^{13}C$ and of 0·1‰ for $\delta^{18}O$.

Mineralogical, TOC and total phosphorus quantification analyses were carried out at the Geological Institute of the University of Neuchâtel, Switzerland. Bulk rock and clay mineral assemblages were analysed using X-ray diffraction (Scintag XRD 2000 Diffractometer; Thermo-ARL, Ecublens, Switzerland) based on procedures described by Kübler (1983) and Adatte *et al.* (1996). The semi-quantification of whole-rock mineralogy is based on XRD patterns of random powder samples by using external standards with an error margin between 5% and 10% for the phyllosilicates and 5% for grain minerals.

Clay mineral analysis follows the methods developed by Kübler (1987) and Adatte *et al.* (1996). The intensities of the identified minerals are measured for a semi-quantitative estimate of the proportion of clay minerals, which is therefore given in relative percent without correction factors, because of the small error margin (<5%).

Total phosphorus quantification analysis was performed on bulk rock samples, following the procedure of Bodin *et al.* (2006) and Mort *et al.* (2007). The concentration of PO_4 in mg l^{-1} with an estimated error margin of <5%, is obtained by calibration with known standard solutions, using a photospectrometer (Perkin Elmer UV/Vis Photospectrometer Lambda 10; Perkin Elmer AG, Scherzenbach, Switzerland). Rock-Eval 6 was performed to obtain oxygen and hydrogen indices (OI and HI), mineral carbon (MinC) and TOC based on methods by Espitalié *et al.* (1985) and Behar *et al.* (2001). Measurements were calibrated using the two standards IFP 160000 and VP143h.

LITHOLOGY

The Azazoul Road outcrop spans from the lower Cenomanian to the base of the lower middle Cenomanian. The Azazoul Beach outcrop encompasses the middle and upper Cenomanian to the base of the Turonian. The basal 3·5 m of the Azazoul Road outcrop consists of burrowed silty and sandy shale layers with a 0·6 m thick limestone and alternating shale and limestone layers (Fig. 2). Above this interval are four oyster-rich limestone beds (3·5 to 28·5 m) separated by nodular laminated shale layers in the lower part (Fig. 2A) and alternating shale and marly limestone layers in the upper part. A 3 m thick dark laminated shale overlies this interval and is terminated by a landslide (Fig. 2B). The top part of the section consists of alternating marly shale and thin limestone layers (Fig. 2C).

The Azazoul Beach outcrop is separated from the road outcrop by a 5 to 10 m landslide (Fig. 3A). The lower part of the section (0 to 31·5 m) consists of alternating shale and marly limestone layers with thin oyster beds (Fig. 3B). Alternating marl and shale layers (31·5 to 45·2 m) with rare nodules terminate in a 0·5 m thick oyster bed. Above are alternating marl and marly limestone beds with ripples in the upper 2 m (46 to 55·6 m; Fig. 4A and B). A shale interval (55·6 to 58·2 m) and alternating marly shale and thin limestone layers (58·2 to 75 m; Fig. 4C) terminate at a 0·6 m thick burrowed limestone with an erosional surface at the top (Fig. 4D and E). Burrows are filled with oyster shell fragments in a fine calcareous matrix originating from the overlying 10 to 20 cm thick layer (75·5 to 76 m) (Fig. 4D and E). This layer shows a grading with larger shell fragments at the bottom and rare small shell fragments to the top. Above,

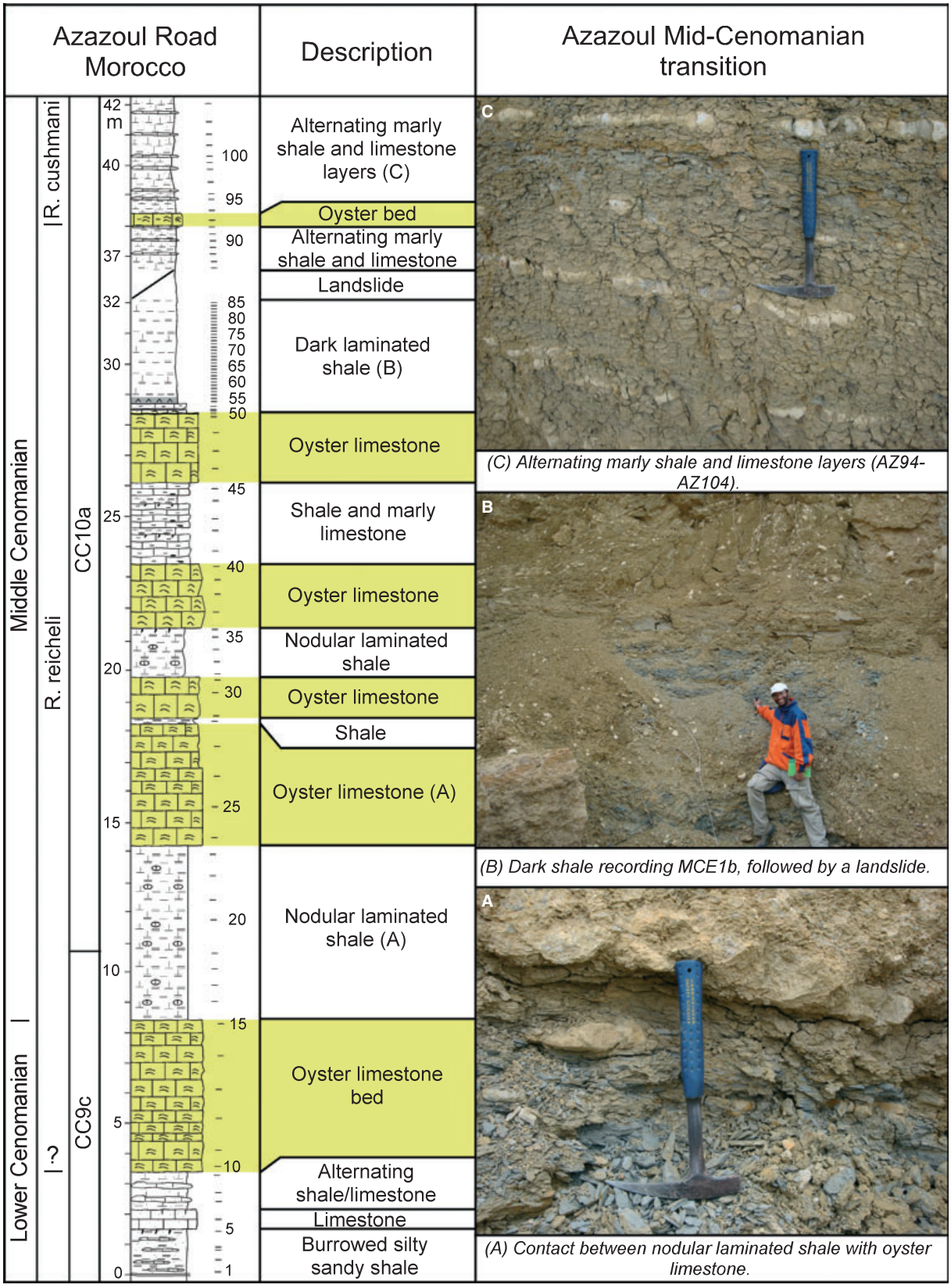

Fig. 2. Lithological description of the Azazoul Road sections with illustrations. Two mid-Cenomanian events MCE1a (17 to 21 m) and MCE1b (27·5 to 32 m) are recorded in this section. See key to lithology in Fig. 3. Hammer for scale in (A) and (C) is 32 cm long. Person for scale in (B) is *ca* 1·8 m tall.

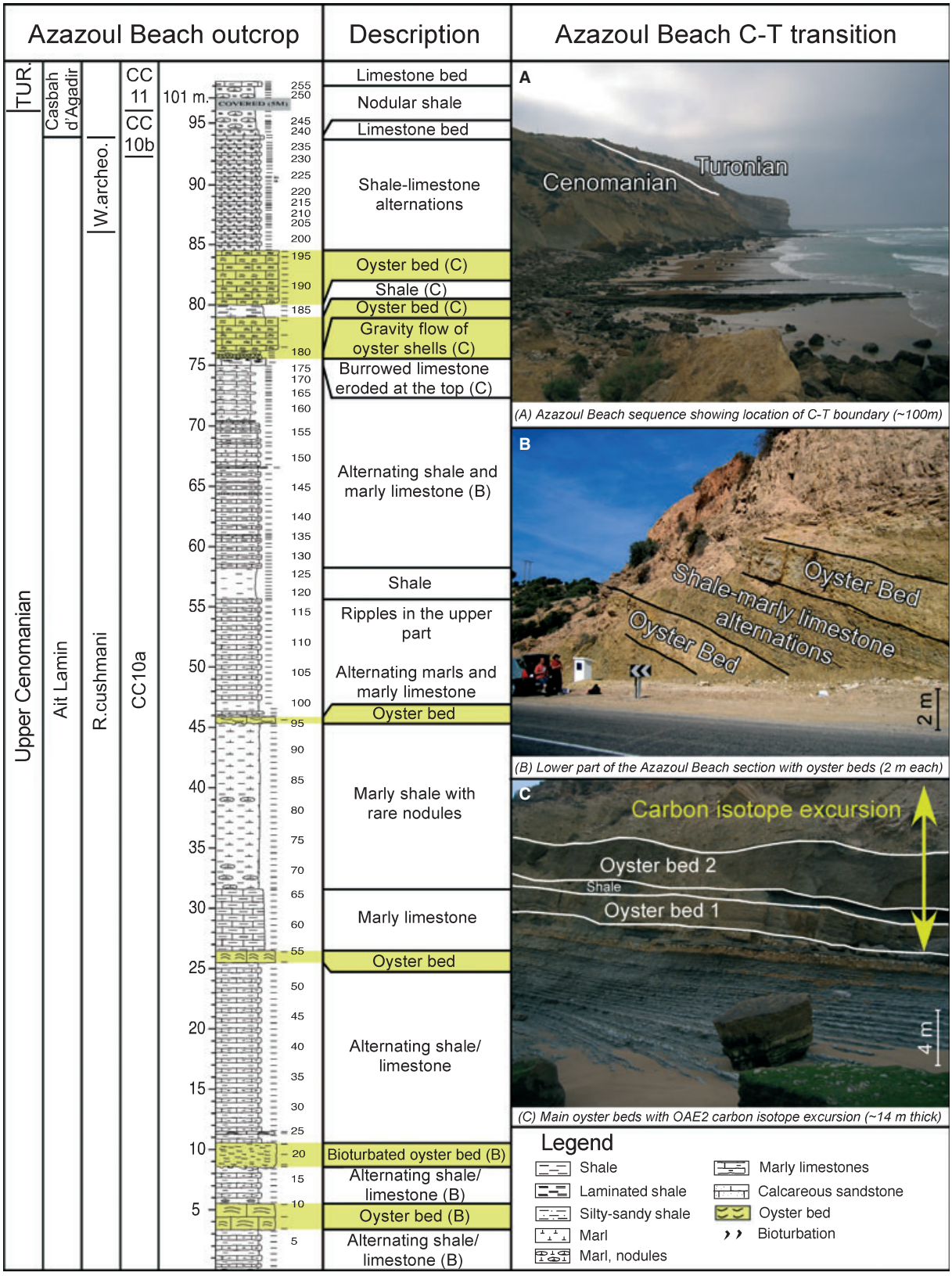

Fig. 3. Lithological description of the Azazoul Beach outcrop with illustrations. Oceanic Anoxic Event 2 (OAE2) spans 76 to 91 m, including the last two oyster beds and the lower part of the alternating marl-limestone layers above.

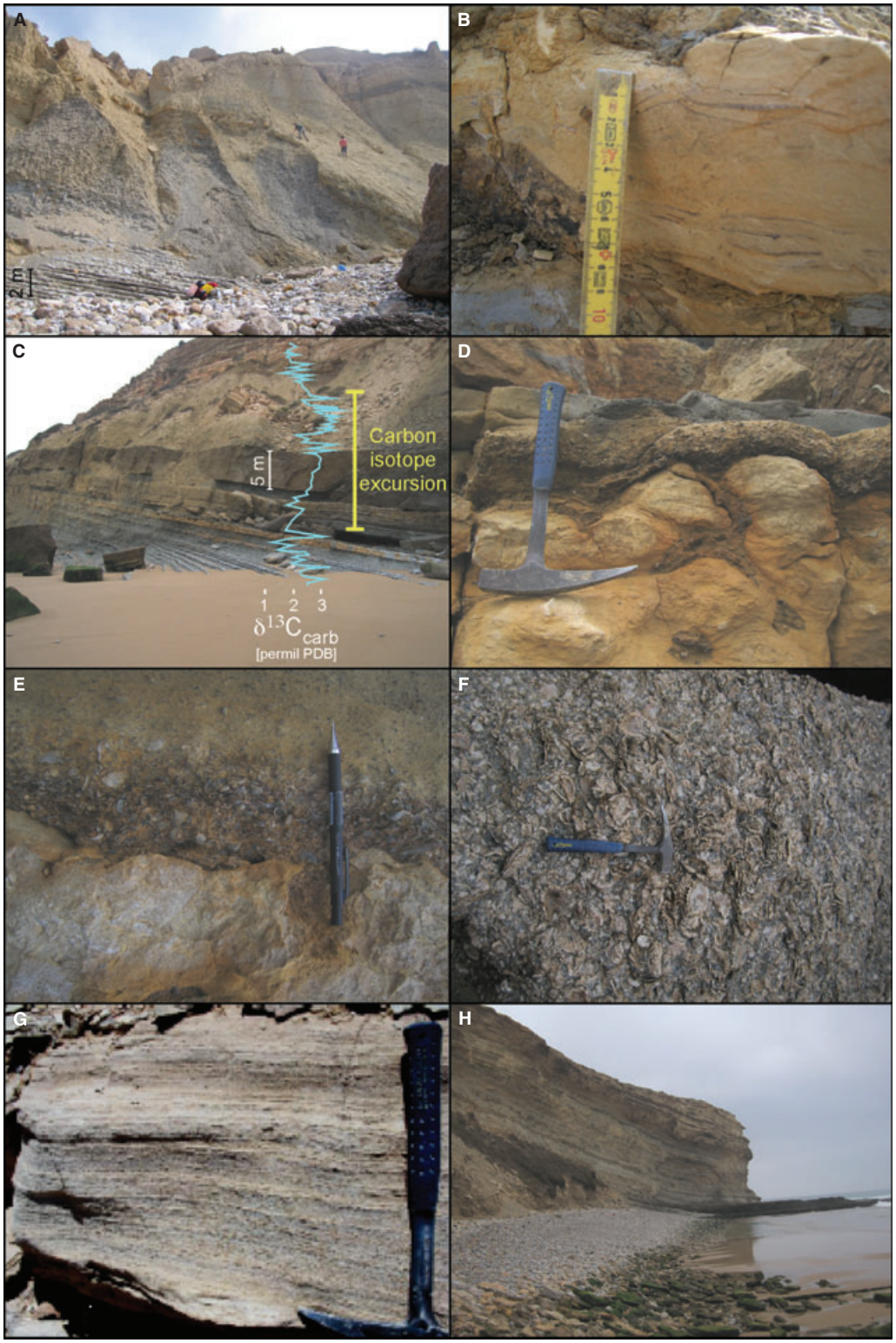

Fig. 4. Characteristic features of the Azazoul Beach section keyed to the lithological column. (A) Alternating marl/marly limestone beds of the middle part (15 to 55 m). (B) Rippled marly limestone beds (53 to 55 m; cm for scale). (C) Interval across OAE2 (73 to 90 m). (D) Unconformity at the top of a bioturbated limestone with burrows infilled by overlying gravity-flow deposit (75·4 to 76 m; hammer for scale is 32 cm long). (E) Contact between the bioturbated limestone and oyster shell gravity flow (75·5 to 75·7 m; pencil for scale is 14 cm long). (F) Oyster limestone bed (76·2 to 79 m; hammer for scale). (G) Early Turonian laminated limestone rich in organic matter (102 to 102·5 m; hammer for scale) (from Jati, 2007). (H) Turonian sequence (*ca* 100 m).

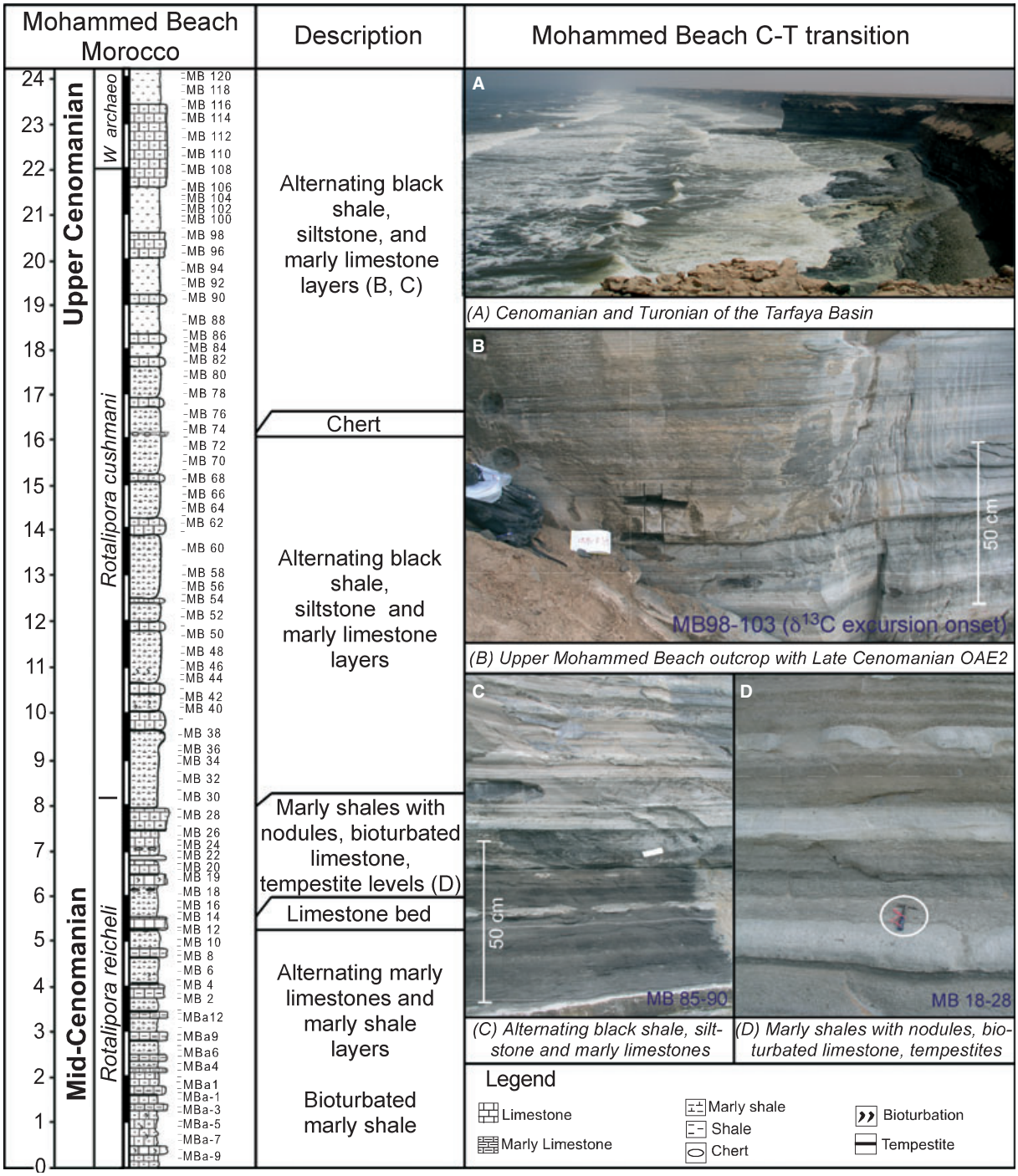

Fig. 5. Lithological description of the Mohammed Beach section with illustrations: (A) Cenomanian–Turonian exposed in cliffs. (B) and (C) Lithological characteristics of OAE2, including alternating black shale, siltstone and marly limestone layers. (D) Alternating nodular shale, bioturbated marly limestone and tempestites from the lower part of the section. Hammer for scale is 32 cm long.

two oyster-rich limestones (76 to 84·5 m) are separated by a 1 m thick shale layer (Figs 3C and 4C, F). Rhythmically bedded thin shale and limestone layers (84·5 to 93·7 m) and organic-rich shale with siliceous nodules mark the top of the outcrop below the landslide (Fig. 4G and H).

At Mohammed Beach deposition occurred in a middle shelf environment of the Tarfaya Basin (Kuhnt *et al.*, 2005, 2009; Mort *et al.*, 2008). The section crops out in the cliffs near Tarfaya and spans the middle Cenomanian to lower Turonian (Fig. 5A). In the lower part of the section (0 to

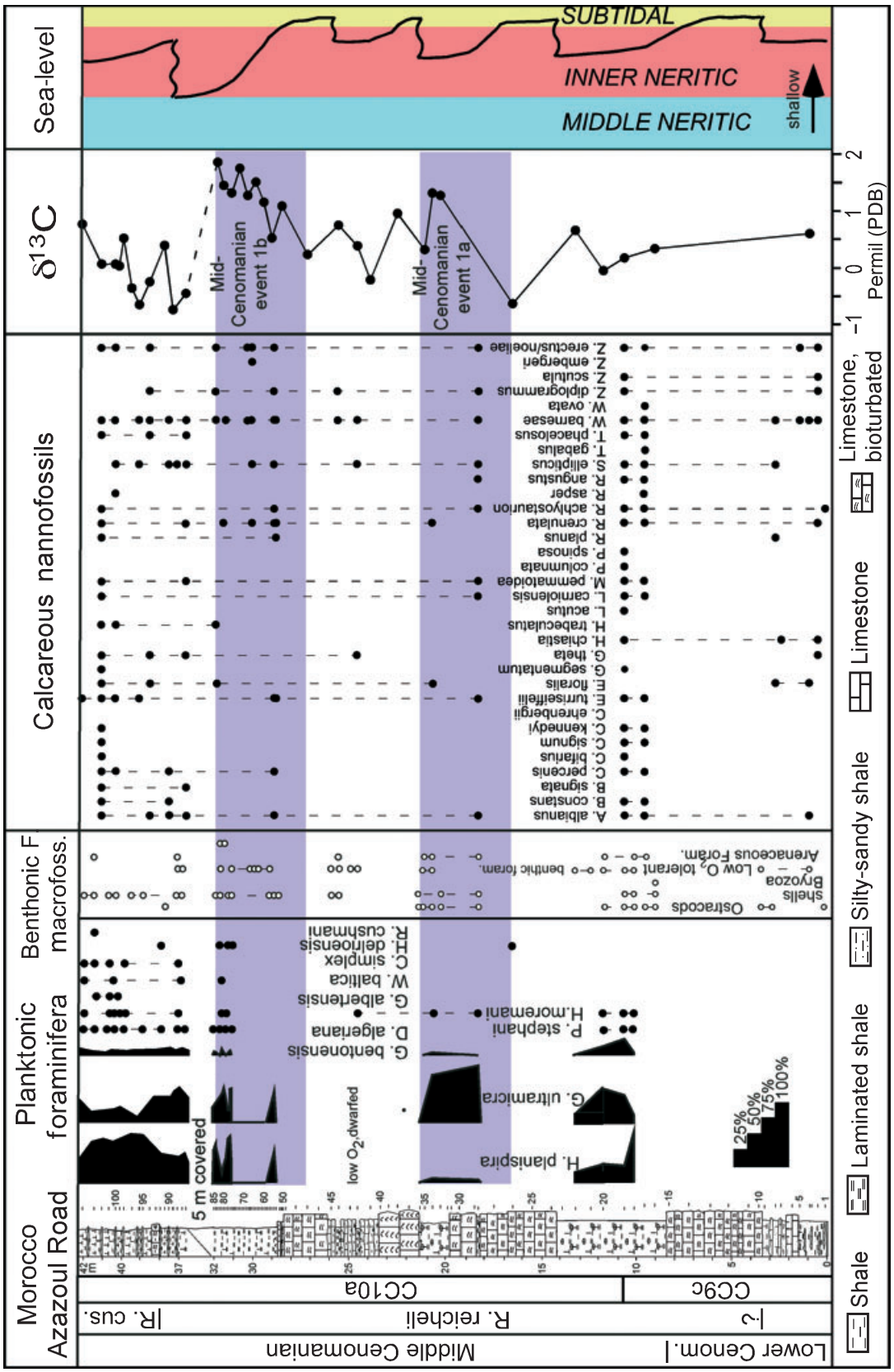

Fig. 6. Early to middle Cenomanian biostratigraphy of planktonic and benthonic foraminifera, macrofossils and calcareous nannofossils with the $\delta^{13}C$ record of the Azazoul Road sequences. Sea-level interpretation is based on lithology, macrofossils (oysters) and foraminiferal assemblages. Note that microfossils are rare or absent in oyster beds and rarely found in silty–sandy shale layers.

5·25 m), 10 to 20 cm thick marly limestone layers alternate with 20 to 70 cm thick marly shale and siltstone layers with bioturbation. Tempestite horizons are observed in the overlying shale and limestone layers are bioturbated (5·25 to 8·0 m; Fig. 5D). Between 8 and 24 m, black shale layers alternate with marly bioturbated limestone and siltstone layers (Fig. 5B and C). A unique 10 cm thick chert layer occurs at 16·2 m (Fig. 5).

BIOSTRATIGRAPHY AND FAUNAL TURNOVER

Planktonic foraminifera generally are rare, although common in specific intervals of the Azazoul section. Wherever present, 100 to 200 specimens were counted. Nannofossil preservation and abundance is also variable. Preservation is generally poor to moderate due to dissolution and calcite overgrowth, as evidenced by high abundance *Watznaueria barnesae* (>50%) (Roth & Krumbach, 1986). Abundance of nannoliths is low (≤1 per field of view), although preservation and abundance improve in the upper part of the section.

Azazoul middle Cenomanian

Calcareous nannofossils and planktonic foraminifera are present sporadically in the relatively deeper water shale intervals and mostly absent in the oyster-rich limestones of the lower to middle Cenomanian Azazoul Road outcrop. In the basal silty-sandy shale layers and limestones (0 to 8 m), planktonic foraminifera are absent and rare nannofossils are restricted to the 2·5 m interval at the base (Fig. 6). The first relatively diverse nannofossil assemblage occurs in the laminated shale interval between 8·4 and 11·5 m, where the first appearance of *Lithraphidites acutus* at 10·5 m tentatively marks the boundary between CC9c and CC10a (Sissingh, 1977; Perch-Nielsen, 1985), or UC2/UC3 of Burnett (1996, 1998). The overlying zone CC10a spans the remainder of the Azazoul Road outcrop (10·5 to 42 m), as indicated by the presence of *Helena chiastia* and co-occurrences of *Axopodorhabdus albianus*, *Corollithion kennedyi* and *L. acutus.*

Small planktonic foraminifera first appear in the bioturbated shale between 10 and 12 m, with assemblages dominated by *Hedbergella planispira*, *Globigerinelloides ultramicra* and *Globigerinelloides bentonensis,* a few *Praeglobotruncana stephani* and *Heterohelix moremani*, but no age diagnostic index species (Fig. 6). Ostracods, bivalves, oysters, bryozoa and low oxygen-tolerant benthonic foraminifera are also present. A similarly impoverished assemblage between 18·5 and 21 m is dominated by *G. ultramicra* and rare nannofossils. Very rare nannofossils and dwarfed (<63 μm) low oxygen-tolerant planktonic (*H. moremani*) and benthonic (*Gavelinella sandidgei, Neobulimina albertensis* and *Pyraminida prolixa*) foraminifera are present in the shale/limestone interval (24 to 26 m). An oyster-rich limestone bed (at 29 m) marks the end of this impoverished interval.

In the alternating thin shale/limestone layers (29 to 32 m) above the oyster-rich limestone bed, planktonic foraminiferal and nannofossil assemblages are more diverse (Fig. 6). *Whiteinella baltica* first appears at the top of this interval, consistent with the middle Cenomanian age (CC10a) of the nannofossil assemblage. A landslide covers the next 5 m of the section. Above the landslide, small planktonic foraminifera are common to abundant and more diverse (for example, *H. moremani*, *Guembelitria cenomana*, *W. baltica*, *Hedbergella delrioensi* and *Clavihedbergella simplex*). The first appearance of the deeper dwelling *Rotalipora cushmani* in this interval reflects the sea-level rise, rather than its evolutionary appearance. Hence, the *Rotalipora reicheli*/*R. cushmani* zone boundary is placed tentatively in the alternating marl/shale interval below the first appearance of *R. cushmani*. The lower part of the section is within the *R. reicheli* biozone, although the index species is not observed due to the shallow environment. This biozone spans the nannofossil CC9c/CC10a boundary (Bralower *et al.*, 1995; Burnett, 1998; Rodriguez-Lazaro *et al.*, 1998). For this reason, the base of the *R. reicheli* zone is placed tentatively below the first major oyster bed (Fig. 6). It is generally observed that the two MCE $\delta^{13}C$ events 1a and 1b fall within the *R. reicheli* planktonic foraminiferal zone and the CC9c/CC10a nannofossil zone (Burnett, 1998; Rodriguez-Lazaro *et al.*, 1998). By contrast, Luciani & Cobianchi (1999) and Coccioni & Galeotti (2003) placed the MCE events within the *R. cushmani* zone in Italy. This discrepancy can be explained by the sporadic presence of *L. acutus* and local conditions in Italy, as suggested by Luciani & Cobianchi (1999).

Azazoul upper Cenomanian

Vegetation covers a 5 to 10 m interval separating the road and beach outcrops of the Azazoul section. The end of the middle Cenomanian interval continues in the bottom part of the

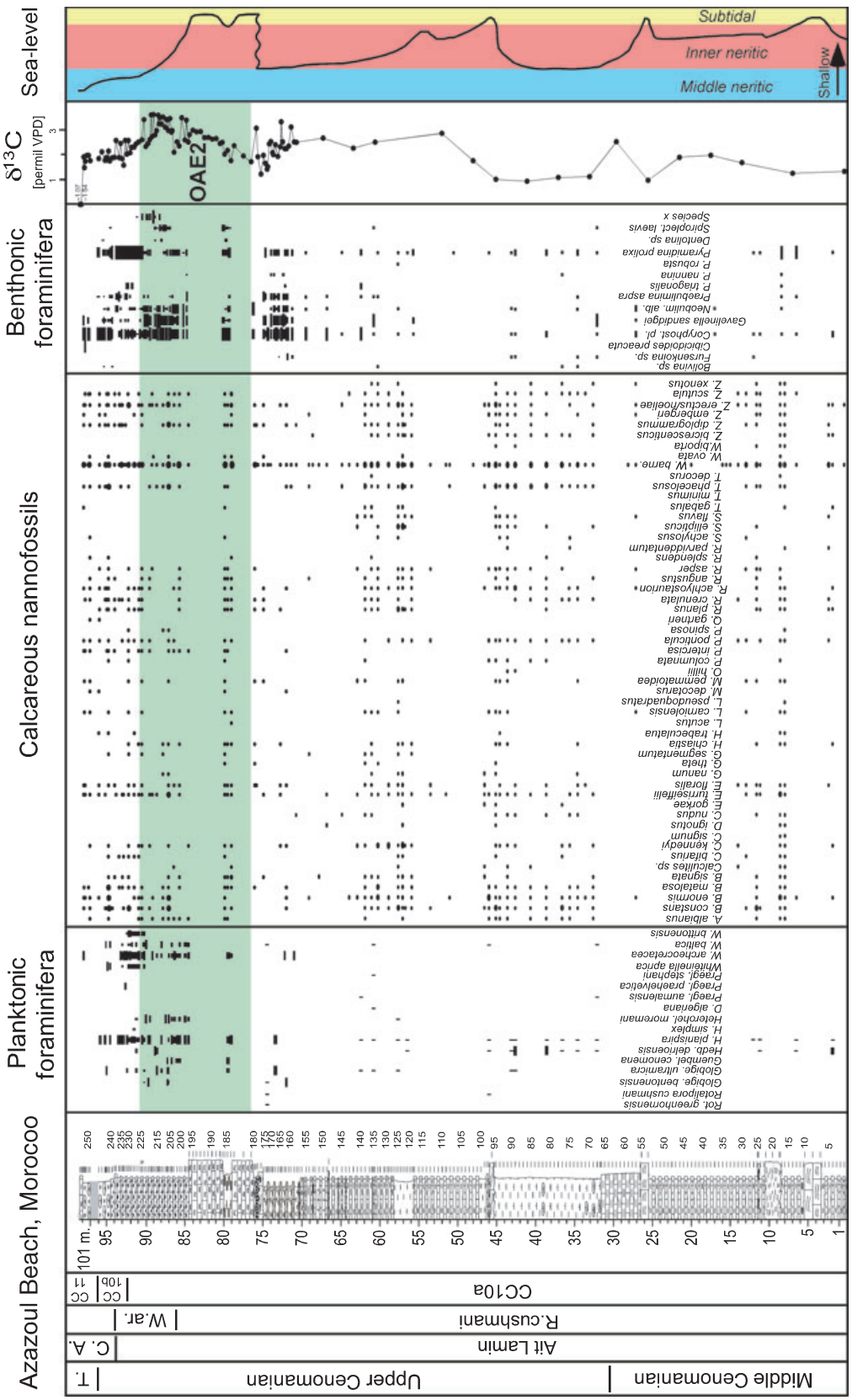

Fig. 7. Middle through to late Cenomanian biostratigraphy of planktonic and benthonic foraminifera and calcareous nannofossils with the $\delta^{13}C$ record of the Azazoul Beach sequence. Sea-level interpretation is based on lithology, macrofossils (oysters) and foraminiferal assemblages.

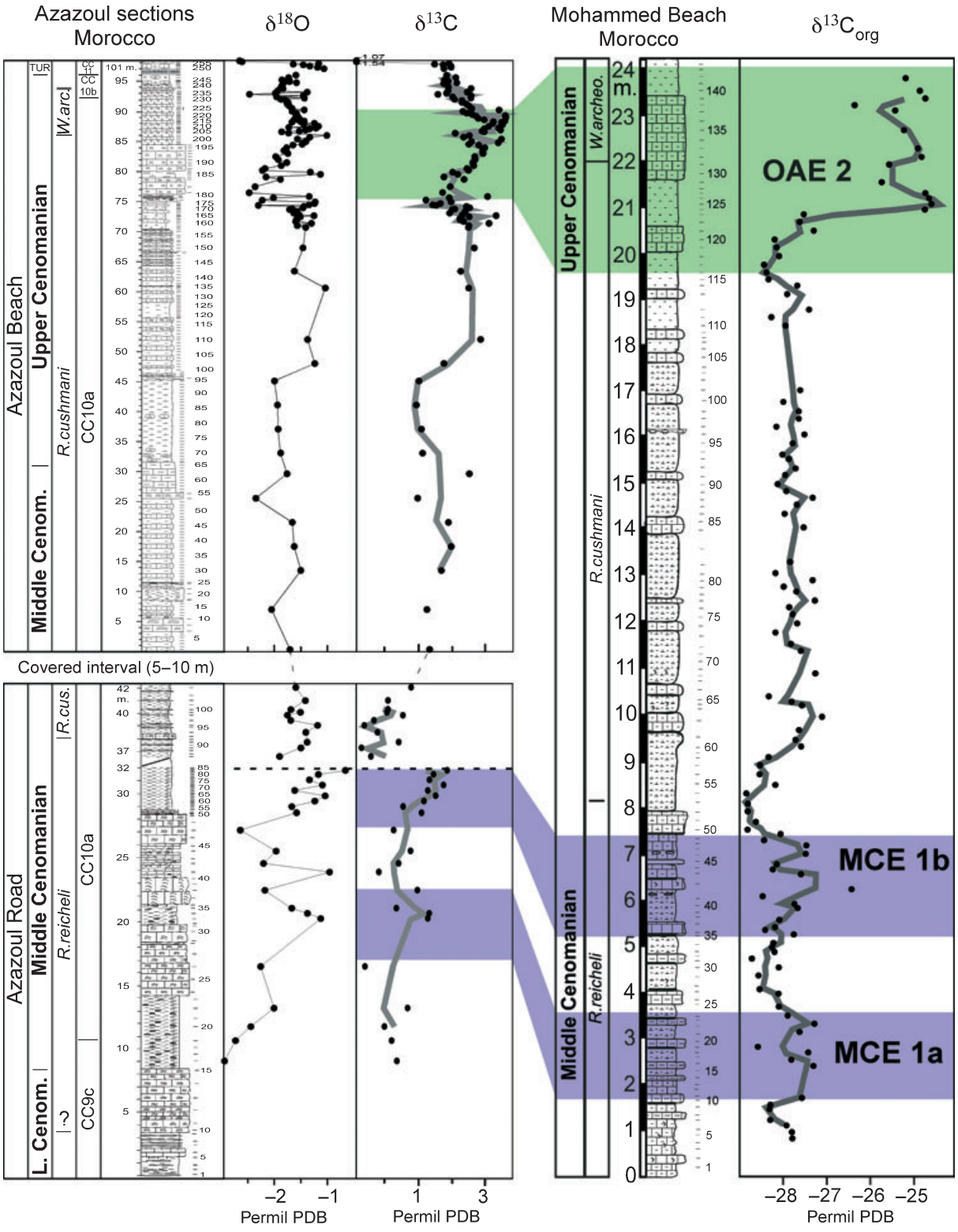

Fig. 8. $\delta^{13}C$ and $\delta^{18}O$ records of the shallow Azazoul sequence correlated with $\delta^{13}C_{org}$ from the deeper Mohammed Beach sequence in the Tarfaya Basin.

Azazoul Beach outcrop (0 to 30 m) and contains sparse foraminiferal assemblages of *H. delrioensis* and *H. planispira* (Fig. 7). Nannofossils are abundant with sporadically high diversity (for example, 8 to 9 m and 11 to 12 m). The boundary between the middle and upper Cenomanian is

placed at the top of the marly limestone interval (30·5 m), just below the first appearance of *Praeglobotruncana aumalensis* and *W. baltica* in the overlying marly shales (31·5 to 45 m).

Similar lithologies and impoverished nannofossil and planktonic foraminiferal assemblages continue into the upper Cenomanian (Fig. 7). Shale and marly limestone layers span most of the upper Cenomanian (31·5 to 76 m), which is marked by an assemblage of *Whiteinella archeocretacea*, *R. cushmani*, *R. greenhornensis*, *P. aumalensis*, *P. stephani* and *Dicarinella algeriana*. Nannofossil assemblages are characteristic of zone CC10a. The prominent oyster-rich limestones (76 to 84 m) generally contain no microfossils. An unknown interval is missing at the erosional unconformity between the limestone and oyster-rich limestones (75·5 m).

Low-diversity small planktonic foraminifera dominate (for example, *G. cenomana, H. moremani* and *H. planispira*) above the last oyster bed (84·5 to 90 m) and a high abundance of the low oxygen-tolerant *Heterohelix* species marks this interval as OAE2 and the *W. archeocretacea* zone (*Heterohelix* sub-zone of Keller *et al.*, 2001, 2008; Keller & Pardo, 2004a). Low oxygen-tolerant benthonic foraminifera dominate this interval (for example, *Coryphostoma plaitum*, *N. albertensis*, *Gavelinella sandigei* and *P. prolixa*; Fig. 7). *Rotalipora cushmani* is absent, making it difficult to place the top of the *R. cushmani* zone. However, this species is known to disappear in the trough between the two δ^{13}C peaks (Keller *et al.*, 2001; Keller & Pardo, 2004a), nearly coincident with the onset of abundant *Heterohelix*, which places this boundary at about 86 m. Increased diversity and abundance of *W. archeocretacea* and decreased abundance of low oxygen-tolerant benthonic species (90·5 to 93·5 m) occur above the *Heterohelix* sub-zone.

Nannofossil assemblages record the last occurrence (LO) of *H. chiastia*, the marker for the CC10a/CC10b boundary at 92·3 m, *A. albianus* at 101 m and *C. kennedyi* at 95·6 m. The simultaneous LOs of *A. albianus* and *H. chiastia* are observed consistently following the disappearance of *C. kennedyi* (Bralower, 1988; Burnett, 1998; Tantawy, 2008). However, in the Azazoul Beach section, *C. kennedyi* seems to disappear above the LO of *H. chiastia* (Fig. 7), which may be due to reworking or the diachronous LO of this species as previously observed in North Africa and Italy (Robaszynski *et al.*, 1990; Luciani & Cobianchi, 1999).

The Cenomanian–Turonian boundary is identified at 96 m by the first appearance of *Quadrum gartneri*, which marks the base of CC11 (=UC7 of Burnett, 1998). The stratigraphically consistent first appearance of *Q. gartneri* near the C/T boundary, as defined by ammonite stratigraphy, and within the δ^{13}C plateau at Pueblo, Colorado (USA), Eastbourne, England, Gubbio, Italy and Tarfaya, Morocco, provides a reliable stratigraphic marker for the C/T boundary and the duration of OAE2 (Tsikos *et al.*, 2004; Kennedy *et al.*, 2006). The planktonic foraminiferal index species for the basal Turonian, *Helvetoglobotruncana helvetica*, was not observed.

Mohammed Beach

At the Mohammed Beach section the *R. reicheli*, *R. cushmani* and *W. archeocretacea zones* were identified, as discussed in Kolonic *et al.* (2005), Keller *et al.* (2008), Mort *et al.* (2008) and Kuhnt *et al.* (2009). The *R. reicheli* biozone spans the lower part of the section up to sample 52, the first appearance of *R. cushmani*. The nannofossil

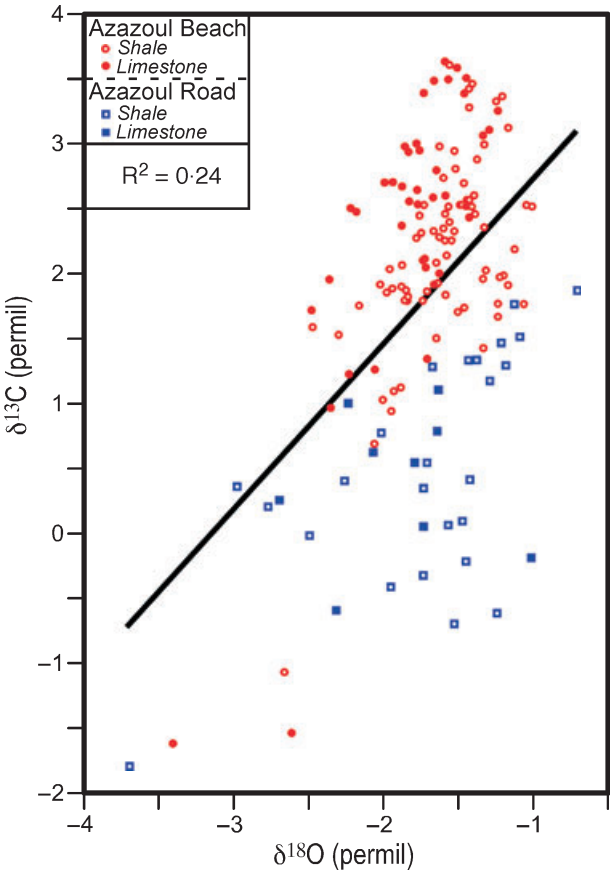

Fig. 9. Cross-plot of the δ^{13}C and the δ^{18}O values of shale and limestone layers from Azazoul Road and Azazoul Beach outcrops. Rare very low diagenetically altered δ^{13}C and δ^{18}O values account for the low correlation factor (R) despite the similar trends observed throughout the section as seen in Fig. 8.

boundary CC9/CC10 coincides with the first mid-Cenomanian event (MCE1a) and the *R. reicheli*/*R. cushmani* zone falls within the trough after the second event, MCE1b (Mort *et al.*, 2008). These results are correlative with the Azazoul biostratigraphy (Fig. 8).

STABLE ISOTOPES

Primary isotopic signals may be altered by post-depositional diagenetic alteration (for example, dissolution, cementation and replacement reactions) rendering them of limited use in palaeoenvironmental interpretations (Jenkyns *et al.*, 1994; Schrag *et al.*, 1995). Oxygen isotopes are more sensitive to diagenetic effects, which may lead to significant lowering of $\delta^{18}O$ values due to recrystallization and/or pore water influence (Schrag *et al.*, 1995). Carbon isotopic values are less prone to alteration during diagenesis due to the low carbon contents of pore waters, but shifts can be important where organogenic carbon is incorporated (Marshall, 1992). Shallow-water carbonates are more likely to undergo diagenesis as a result of meteoric-vadose diagenetic overprinting. However, various studies have demonstrated that the $\delta^{13}C$ records of Cretaceous shallow-water sections with strong diagenetic overprinting can be correlated with well-preserved deep-water sections (Jenkyns, 1991; Grotsch *et al.*, 1998; Davey & Jenkyns, 1999; Buonocunto *et al.*, 2002; Parente *et al.*, 2007).

A cross-plot of carbon and oxygen isotope values of the Azazoul section shows no significant trend (R^2 = 0·24; Fig. 9). Most $\delta^{18}O$ and $\delta^{13}C$ values fall in the range of −3·7‰ to −1·2‰ and −2‰ to 3·5‰, respectively, and no distinctive trends due to limestone or shale lithologies are apparent (Fig. 9). The relatively constant $\delta^{18}O$ values (−2·5‰ to −1‰) suggest only minor diagenetic overprinting, except on rare single samples. Nevertheless, carbon and oxygen isotope curves show parallel trends, except for single peaks and short excursions (Fig. 8), which apparently account for the low R^2. Therefore, oxygen isotopes are probably affected by diagenesis, although general temperature trends may be preserved. Thus, oxygen isotopes will not be discussed further.

Middle Cenomanian events MCE1a and MCE1b

In the lower to middle Cenomanian of the Azazoul section (0 to 16·5 m) few samples contained sufficient carbonate for stable isotope analysis and these show very low $\delta^{13}C$ (−0·6‰ to 0·6‰) values. A $\delta^{13}C$ excursion to 1·2‰ is restricted to a 1·5 m thick shale/marl interval (20 to 21·5 m) between the 6 and 1·5 m thick oyster-rich limestone beds below and above, respectively. This $\delta^{13}C$ excursion probably marks the first mid-Cenomanian event (MCE1a). In the oyster-rich limestone above 22·5 m, a $\delta^{13}C$ value of 1‰ suggests that the excursion persisted through this interval.

The second mid-Cenomanian $\delta^{13}C$ excursion (MCE1b) occurs in the alternating shale and marl layers (29 to 32 m). In this interval, $\delta^{13}C$ values increase gradually from −0·5‰ to 1·9‰ (Fig. 8). The full excursion cannot be documented because a landslide covers about 5 m of the section that presumably details the nearly 3‰ decline evident above the landslide.

At the Mohammed Beach section, the high organic content in the middle and upper Cenomanian rocks necessitated analysis of organic carbon isotopes. In the middle Cenomanian, $\delta^{13}C_{org}$ values increased from −27·8‰ to −27·4‰ and remained steady up to 3·2 m (Fig. 8). This interval marks MCE1a. A second $\delta^{13}C_{org}$ excursion, which marks MCE1b, begins with a gradual increase at 5 m, reaches a maximum of −26·5‰, and is followed by a decrease to minimum values at 8 m (−28·8‰; Fig. 8).

Late Cenomanian OAE2

At Azazoul Beach, $\delta^{13}C$ trends show small fluctuations between 0 and 75 m with gradually decreasing values in $\delta^{13}C$ in the last 5 m. $\delta^{13}C$ reaches a minimum just below the erosional unconformity at the base of the limestone (Fig. 8). Excluding the anomalous peak value at the unconformity, $\delta^{13}C$ values increase gradually from 1·2‰ to 3‰ through the oyster-rich limestone (75·5 to 84 m) and reach the first OAE2 excursion maximum of 3·4‰ at the base of the alternating shale/limestone interval (84·5 m). A drop in $\delta^{13}C$ values to 2·1‰to 2·5‰ (85·5 to 86·5 m) forms a short trough, overlain by an abrupt shift to 3·7‰, which marks the onset of the second OAE2 $\delta^{13}C$ excursion. High $\delta^{13}C$ values persist between 86·5 and 88·5 m, after which $\delta^{13}C$ values decrease gradually to around 2‰ across the C/T boundary. At the top of the section, a drop in $\delta^{18}O$ and $\delta^{13}C$ values in the marly limestone is probably due to diagenetic effects and/or enriched OM in the laminated shale of the lower Turonian.

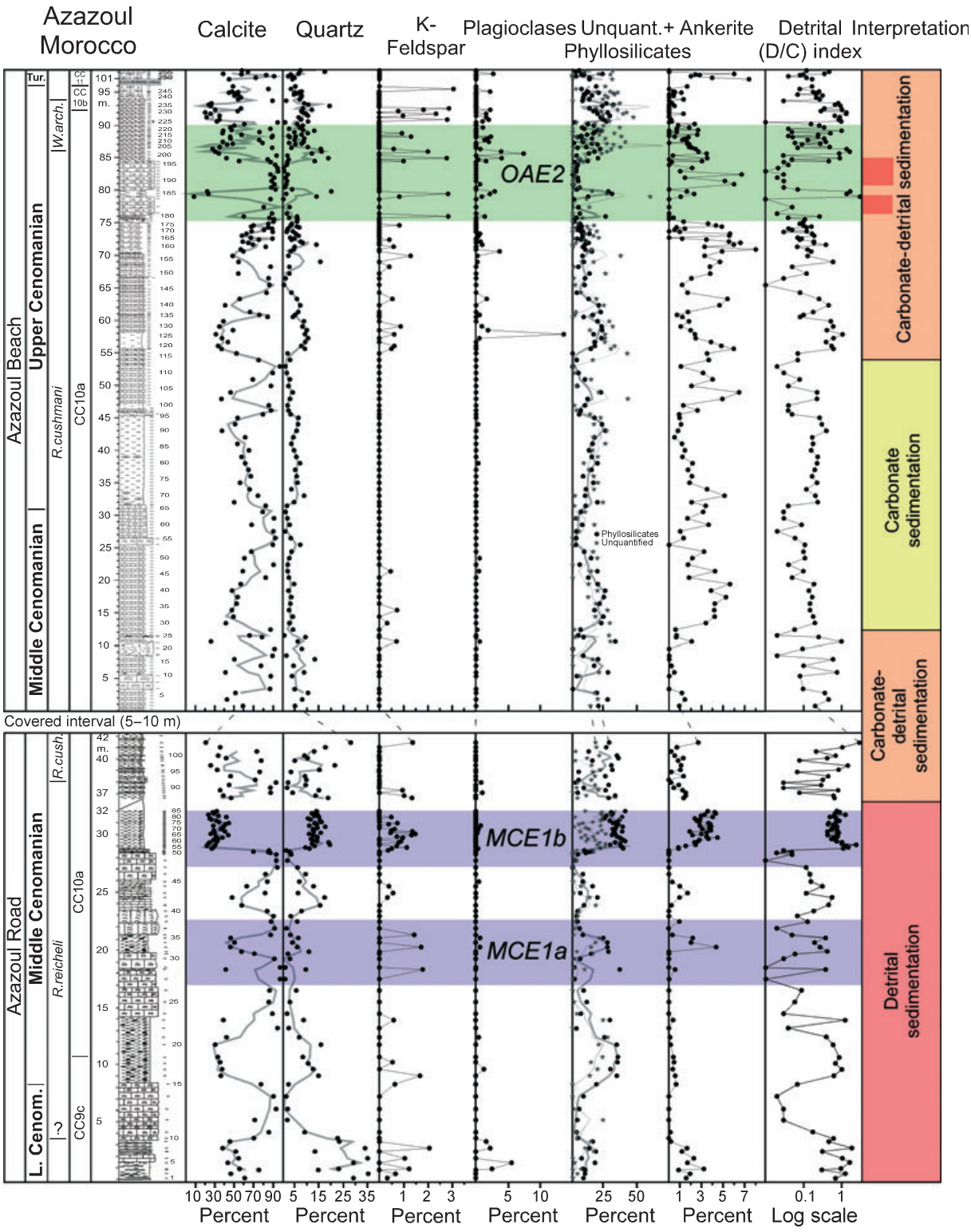

Fig. 10. Bulk rock analysis of the Azazoul section. Grey lines mark three-point moving average for calcite, phyllosilicates and unquantified. Oyster beds are dominated by high calcite and high detrital influx. Unquantified minerals include a non-identified group of organic material and poorly crystallized minerals.

At Mohammed Beach the drop in $\delta^{13}C_{org}$ values above MCE1b is overlain by a gradual increase to plateau around MCE values, as also observed at Azazoul Beach. Above this increase, $\delta^{13}C_{org}$ values remain relatively steady up to the OAE2 carbon isotope excursion, which is marked by a

sudden shift to peak values of −24·7‰ (20·5 m; Fig. 8). Lower values (−25·8‰, 21·5 m) form a trough with a second peak of −24·9‰ (22 m) and high $\delta^{13}C_{org}$ values persist to the top of the section.

MINERALOGY

Bulk mineralogy

Azazoul section

Calcite, quartz and phyllosilicates dominate the Azazoul section, although values are highly variable and reflect the alternating shale/limestone layers, oyster beds and marly limestones. In the lower to middle Azazoul Road outcrop calcite dominates in the marl/limestone intervals (40% to 70%) and oyster beds (70% to 90%) with lower values in shale, whereas phyllosilicates show the opposite pattern with high values in shale (Fig. 10). Quartz content is the highest for the section at the base (35%), about 15% to 20% in shale and <5% in limestone and oyster beds. K-feldspars are variably present (0% to 2%), ankerite is restricted to three shale layers and plagioclase is rare with peaks in the basal part (up

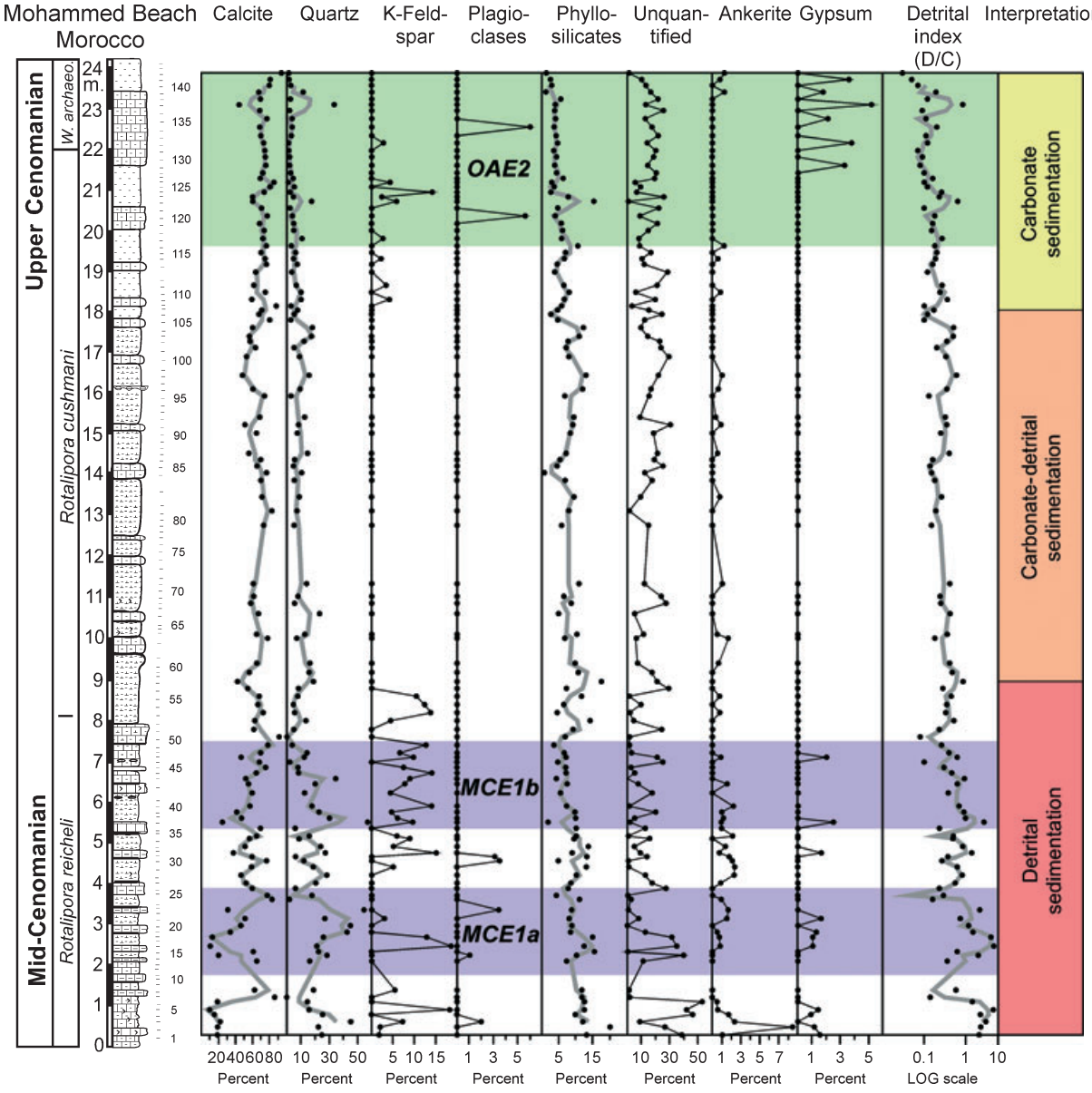

Fig. 11. Bulk rock analysis of the Mohammed Beach section. Grey lines mark three-point moving average for calcite, quartz, phyllosilicate and detrital index. Calcite increases steadily upsection, whereas detrital minerals (quartz, phyllosilicate, plagioclases and K-feldspar) decrease, reflecting a change from detrital to carbonate-dominated sedimentation.

to 5%) (Fig. 10). The detritus/calcite (D/C = (quartz + phyllosilicates + K-feldspars + Na-plagioclase)/calcite) index reflects the low detrital influx at times of oyster deposition and high influx during shale deposition.

At Azazoul Beach calcite dominates limestones and oyster beds (90%) but shows lower values in shale layers, which are dominated by phyllosilicates (Fig. 10). Quartz content is significantly lower (<5%) than in the underlying middle

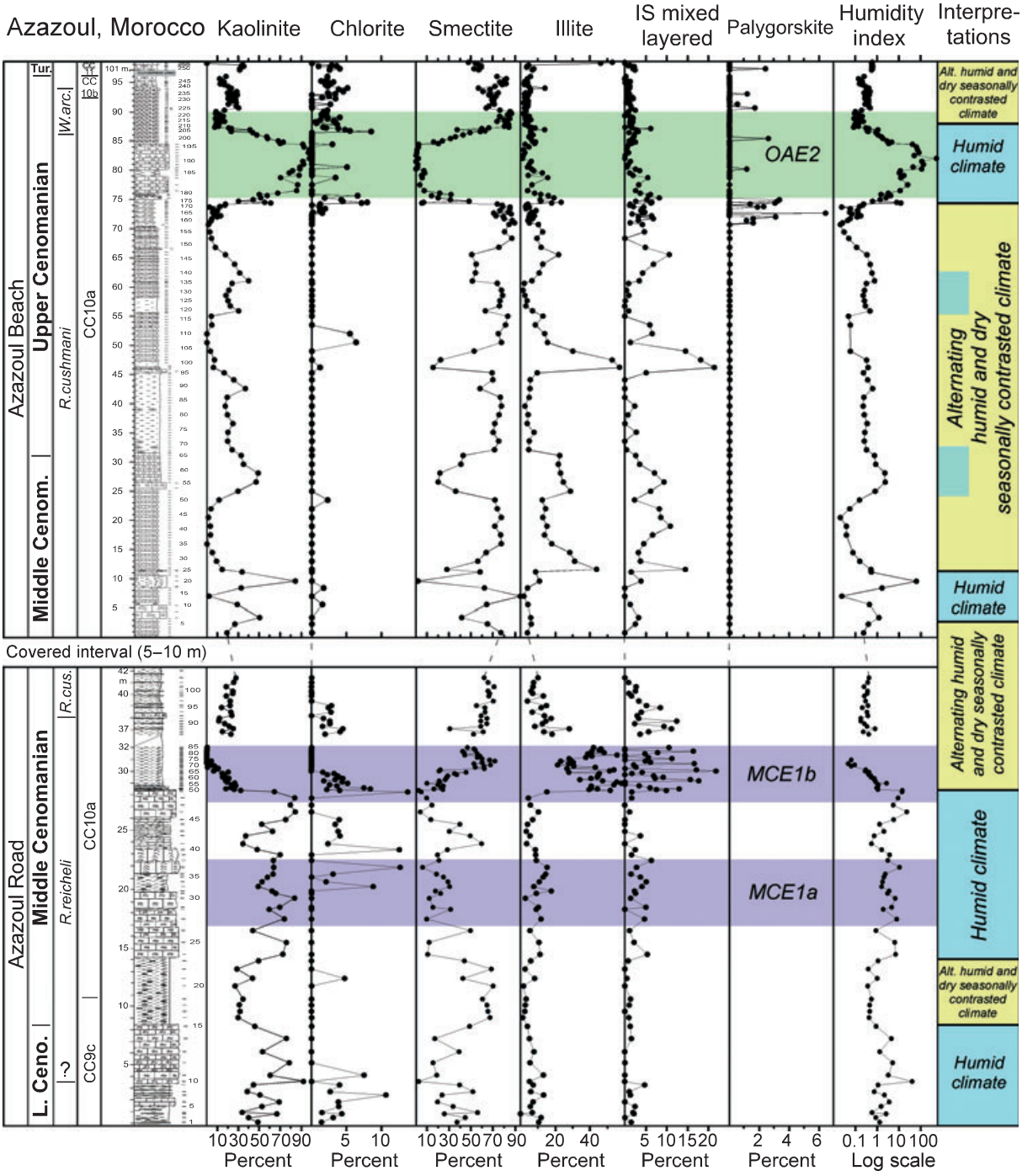

Fig. 12. Clay mineralogical analysis of the Azazoul section. Dominant kaolinite content marks humid conditions up to 29 m at the Azazoul Road outcrop. Dominant smectite suggests dry and seasonally contrasted conditions in the upper Azazoul section but interrupted by locally humid conditions, as indicated by high kaolinite contents (Azazoul Beach: 4 to 10 m and 75 to 84 m).

Cenomanian, except for the shale at the base of the section (55 to 60 m) and shale layers associated with the OAE2 excursion (Fig. 10). Scattered plagioclase and K-feldspar peaks appear in the upper part of the section (55 to 100 m). Compared with the middle Cenomanian, ankerite is high, but variable in shale layers and low in the carbonate-rich intervals. The detritus/calcite values continue the trend of the underlying road section with higher ratios (0·5 to 2) in the marl/shale layers, and low ratios in limestone and oyster beds (<0·1).

Mohammed Beach section

Bulk rock minerals at Mohammed Beach are less variable than at Azazoul. Calcite is the dominant mineral and varies between 60% and 95% throughout most of the section, but concentrations are sporadic with low values near the base (0 to 1, 2 to 3 and 3·5 to 8·5 m), where quartz reached 50%, K-feldspar 15% and unquantified minerals 40 to 50% (Fig. 11). Quartz decreases steadily upsection to <5%, K-feldspar is absent but reappears below the OAE2 excursion, and the unquantified content varies between 0% and 30%. Phyllosilicate content is low and decreasing steadily upsection from 15% to 20% to <5% at the top. Plagioclase is absent, except for some isolated peaks. Ankerite content is <3% in the lower part of the section and nearly absent upsection. Isolated occurrences of late diagenetic gypsum are present near the top of the section and in the lower part. The detrital index is the highest and most variable (0·1 to 10; average of 1) in the lower part of the section (0 to 8 m) and decreases steadily upsection.

Clay mineralogy

Azazoul section

Clay assemblages consist of kaolinite, chlorite, smectite, illite and illite–smectite (IS) mixed layers. At the Azazoul Road outcrop (Fig. 12), kaolinite dominates the lower part of the section (0 to 28·5 m; 60% to 90%), except for lower values (30% to 40%) in shale, marl and marly limestone intervals where smectite is the main clay mineral (50% to 80%). Kaolinite is nearly absent in the shale below the landslide. Smectite also dominates the upper part (30 to 42 m). Illite and IS mixed layers show similar patterns with steady, low values throughout the lower part of the section, increasing only in the shale (28·5 to 30 m, 40% to 80%) and gradually returning to lower values at the top (Fig. 12). Chlorite shows sparse peaks (up to 14%) throughout the road outcrop. The kaolinite/smectite ratio is a humidity index (Chamley, 1989; Pardo *et al.*, 1999; Adatte *et al.*, 2002), which shows high ratios (1 to 20) in the lower 28·5 m of the section and lower ratios (0·1 to 1) in the upper part (28·5 to 42 m).

At the Azazoul Beach outcrop (Fig. 12), smectite is the main clay mineral (80% to 90%), except in oyster beds and marly limestones (26·5 to 31·5 m) where kaolinite dominates (50% to 90%). Transitions between smectite-dominated to kaolinite-dominated intervals are gradual over 1 to 2 m. Chlorite and palygorskite show scattered peaks up to 8%. Illite and IS mixed layers show similar trends with generally low values, except in some intervals (11 to 31·5 m, 46 to 55·5 m; 62 to 71 m) where values can reach 55% and 20%, respectively. The kaolinite/smectite ratio is low, but variable, for most of the section (0 to 74 m) with maximum values (1 to 100) in two large oyster beds (76 to 79 m and 80 to 84·5 m, Fig. 12). Above the oyster beds values decrease gradually to a steady 0·8 ratio.

Mohammed Beach

Clay mineral assemblages at Mohammed Beach consist mainly of smectite, IS mixed layers, kaolinite and illite, with chlorite only as a minor component (Fig. 13). The lower part of the section (0 to 4·5 m) is dominated by illite (20% to 70%) and kaolinite (10% to 50%), with minor chlorite (2% to 7%), smectite (<35%) and IS mixed layers (<5%). Between 4·5 and 8·0 m smectite increases gradually to 80% as illite decreases to 10% and kaolinite disappears. Between 8·0 and 18·0 m, smectite and illite are highly variable at lithological changes, with smectite decreasing gradually to 5% and illite increasing (Fig. 13). In the top part of the section (18 to 24 m), smectite remains low but variable, whereas illite increases only near the top (22 to 24 m). The low smectite and illite values are accompanied by high IS mixed layer components (Fig. 13) but, for most of the section, IS mixed layers remain low (<20%, Fig. 13).

ORGANIC CARBON AND PHOSPHORUS

Organic carbon

Rock-Eval pyrolysis data from the upper part of the Azazoul section indicate very low average TOC values (0% to 0·3%), but reach 0·6% and 1% in the last two samples at the top of the section

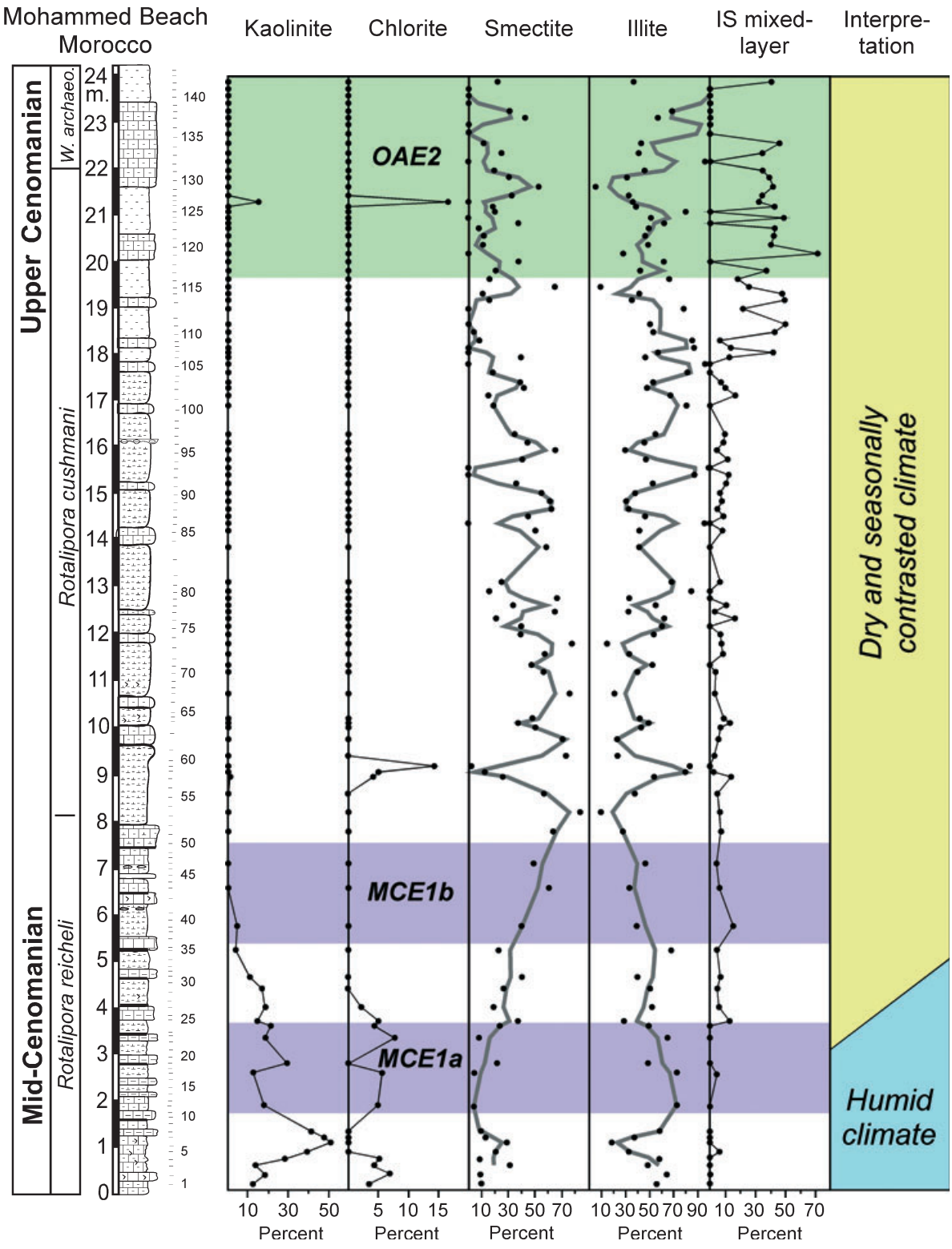

Fig. 13. Clay mineralogical analysis of the Mohammed Beach section. Dominant kaolinite at the bottom of the section marks humid conditions. Dominant smectite and illite in the rest of the section suggest dry and seasonally contrasted conditions.

(Fig. 14). Total organic carbon values are at a minimum in the oyster-rich limestone. The origin and maturity of the OM can be deduced by pyrolytic measurements (Espitalié *et al.*, 1985;

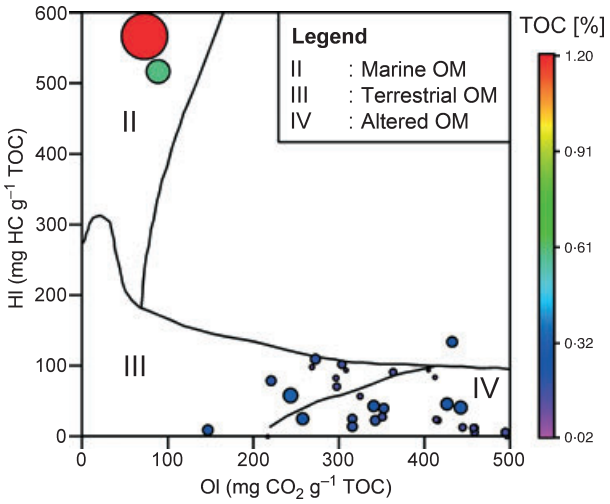

Fig. 14. Oxygen index (OI) versus hydrogen index (HI) diagram of organic matter (OM) in the Azazoul section shows that organic matter consists mostly of altered and terrestrial origins, except for two samples that indicate a marine origin.

Behar *et al.*, 2001). Determination of the HI and OI allows the characterization of the type of OM. At Azazoul Beach, OM is mainly altered (type IV; Fig. 14). High OI values (>300 CO_2 per g TOC) and low HI (100 to 150 mg HC per g TOC) values reflect significant alteration and oxidation of OM. Few samples contain terrestrial OM (OI < 300 CO_2 per g TOC and HI between 100 and 150 mg HC per g TOC). The last two samples of the Azazoul section indicate organic matter of marine origin (OM type II) with a high hydrogen index and low oxygen index. (Fig. 14).

At Mohammed Beach, OM preservation is good and of marine origin. Total organic carbon contents vary between 1% and 5% in the lower part of the section (0 to 8·5 m), whereas HI varies between 220 and 700 mg HC per g TOC (Fig. 15). Between 8·5 and 21 m, TOC remains between 2% and 8% up to the onset of the $\delta^{13}C$ shift (average: 5%) and HI values stabilize around 700 mg HC per g TOC. The uppermost part of the section (21 to 24 m) shows the highest values (6% to 10%), while HI values are scattered (400 to 750 mg HC per g TOC) and average 600 mg HC per g TOC.

Total phosphorus concentration

Total phosphorus (P) concentrations show values from 100 to 1700 p.p.m. for the Azazoul Road and Azazoul Beach outcrops (Fig. 15). In the lower to middle Cenomanian road outcrop, P concentrations are low and constant (100 to 500 p.p.m.), except in five levels with isolated peaks at lithological boundaries. In the middle to upper Cenomanian beach outcrop, a similar pattern is repeated with single peak high values coinciding with lithological boundaries. These anomalous peaks most likely mark reworking and concentration of P.

At Mohammed Beach, total P was analysed from 2 m below the $\delta^{13}C$ excursion to the top of the section (Fig. 15). Below the $\delta^{13}C$ excursion, total P concentrations are variable but usually high (up to 1400 p.p.m.). During the $\delta^{13}C$ excursion total P concentrations remain low.

DISCUSSION

Sea-level

Sea-level fluctuations in the Azazoul section can be inferred from lithological changes (oysters and marl-limestone alternations) and the foraminiferal record. Oyster beds consist of 1 to 5 m thick biostromes and extend laterally over several hundreds of metres. Cenomanian strata of Morocco (Andreu, 1989), Sinai (Bauer *et al.*, 2001; Gertsch *et al.*, 2010) and Jordan (Schulze *et al.*, 2003, 2004, 2005) are marked by the presence of extensive oyster biostromes, which formed a specific facies in the Tethys and North Africa (Dhondt *et al.*, 1999).

High energy, shallow and faunally restricted environments with low salinity, mesotrophic nutrient level and a turbid water column are characteristic palaeoenvironmental conditions for oyster build-ups (Glenn & Arthur, 1990; Pufahl & James, 2006). These conditions are encountered in shallow sub-tidal (<20 m) and estuarine environments (Trappe, 1992; Dhondt *et al.*, 1999; Pufahl & James, 2006), such as the Atlas Gulf, where Azazoul was located during the Cenomanian. Thus, the frequent oyster-rich limestones in the early and middle Cenomanian indicate sub-tidal environments alternating with drowning of oyster biostromes marked by the influx of low-diversity planktonic foraminiferal and nannofossil assemblages. This effect is also indicated by the high abundance of low oxygen-tolerant benthonic foraminifera in shale layers, dominated by *C. plaitum*, *G. sandidgei* and *N. albertensis* in the shale layers but absence in oyster-rich limestones (Fig. 6).

The Cenomanian to early Turonian is characterized by a major global transgression (Haq *et al.*, 1987; Gale *et al.*, 2008; Müller *et al.*, 2008) superimposed by fluctuating sea-levels (Sageman *et al.*, 2006; Sahagian *et al.*, 1996; Gale *et al.*,

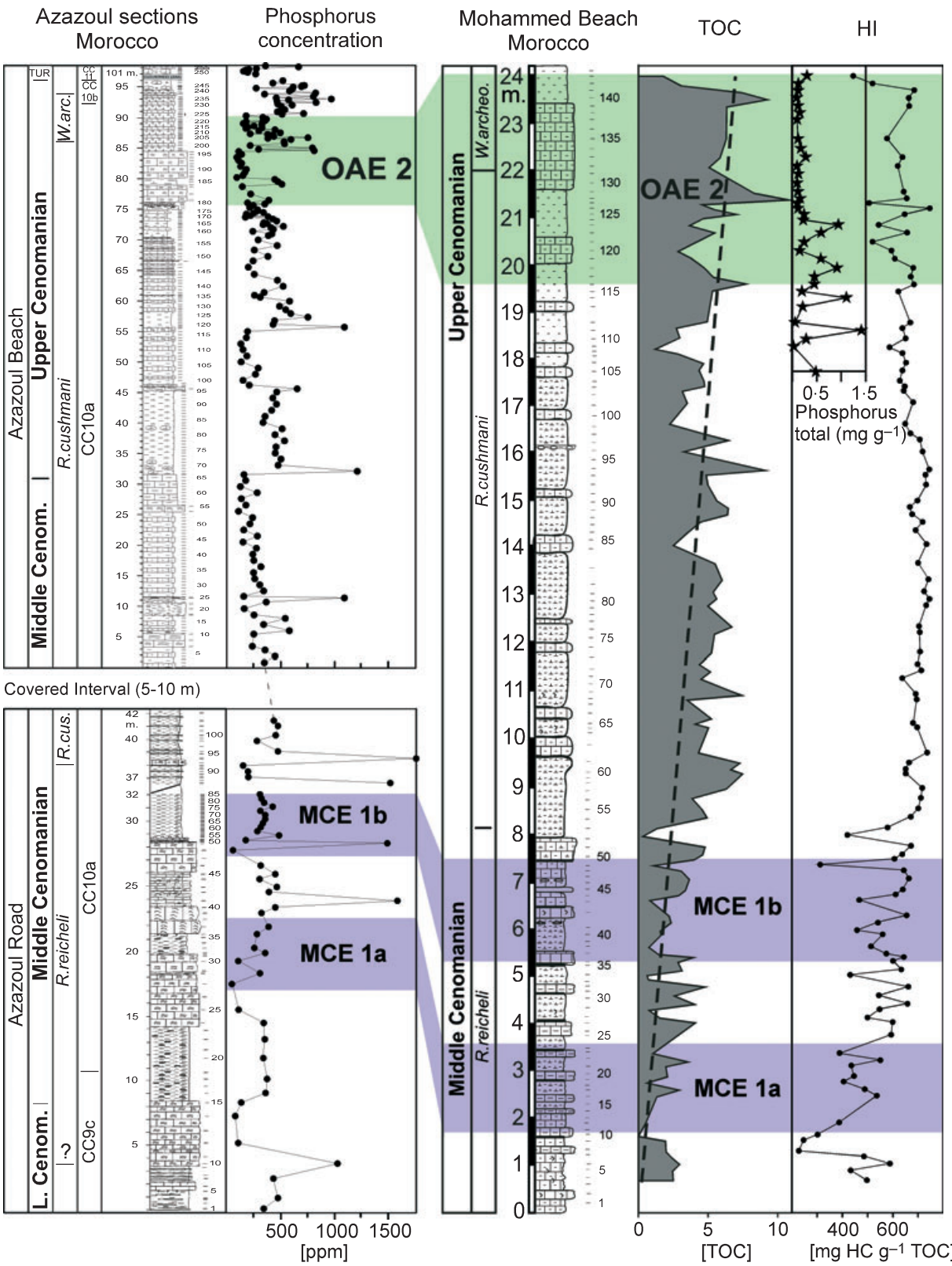

Fig. 15. Phosphorus concentrations of the Azazoul section compared with phosphorus (P), total organic carbon (TOC) and hydrogen index (HI) at Mohammed Beach.

2002, 2008). During the early Cenomanian, sea-level steadily increased followed by a major sea-level fall at the early/middle Cenomanian boundary (MCE1a) and a rapid sea-level rise (Gale *et al.*, 2002, 2008). Similar sea-level trends can be observed at Azazoul during the early to middle Cenomanian, including low-amplitude, short-term sea-level falls leading to oyster deposition (Fig. 6).

During the late Cenomanian, this major sea-level rise is observed at Mohammed Beach by decreasing detrital influx and increasing HI values (Figs 11 and 15). However, the Morocco record also shows several short, low-amplitude sea-level changes, which are not all recognized in the global eustatic sea-level curve (Hardenbol *et al.*, 1998; Gale *et al.*, 2002, 2008) (Fig. 7). The most noticeable sea-level fall is observed in both Azazoul and Mohammed Beach sections prior to OAE2. A small tempestite or gravity-flow marks the sea-level low at Azazoul. The tempestite contains reworked oyster shells from sub-tidal to inner neritic environments and is correlative with the abrupt $\delta^{13}C$ change in the condensed interval below OAE2 at Mohammed Beach. This sea-level fall is also recorded in shallow sequences of Central Europe with an estimated 5 to 10 m decrease prior to OAE2 (Gale *et al.*, 2002; Wilmsen, 2003; Voigt *et al.*, 2006).

Palaeoclimate

The formation of clay minerals in terrestrial soils depends on the type of rocks and climatic conditions. Kaolinite and smectite are the major clay components. Kaolinite forms under humid conditions in equatorial soils, whereas smectite forms by alteration of basalts, or in tropical soils under dry, seasonal climate conditions (Adatte & Rumley, 1989; Chamley, 1989; Chamley *et al.*, 1990; Deconinck & Chamley, 1995). Apart from climate, the distribution of clay minerals is influenced by authigenesis (Chamley, 1989; Kübler & Jaboyedoff, 2000) and the differential settling of kaolinite versus smectite (Thiry, 2000; Godet *et al.*, 2008). Authigenesis, which refers to the recrystallization of new minerals during diagenetic processes, is generally associated with tectonic activity and/or burial depth. In the Azazoul and Mohammed Beach sections the weak tectonic activity and the shallow burial depth eliminate authigenesis as a significant factor.

Differential settling of clay minerals is caused mainly by physical segregation of clay particles, such as the smaller size of smectite relative to illite, kaolinite and chlorite (Chamley, 1989). Thus, larger clay particles (for example, illite, kaolinite and chlorite) settle preferentially closer to the coast and in platform environments, whereas smectites are carried into basins or offshore. In the marine clay record differential settling of clay minerals is therefore defined by the positive correlation between kaolinite, chlorite and illite contents in the most proximal section (Chamley, 1989). Applying this concept, differential settling can be evaluated based on clay mineral assemblages of the shallow-water Azazoul section. No correlation between kaolinite, chlorite and illite contents ($R^2_{\text{kaol-chlo}} = 0{\cdot}005$; $R^2_{\text{kaol-illite}} = 0{\cdot}05$; $R^2_{\text{chlo-illite}} = 0{\cdot}002$) is observed, which therefore indicates the absence of differential settling.

A similar lack of correlation was observed by Godet *et al.* (2008) based on the Vocotian trough during the Hauterivian with sections 500 km apart. In this area, clay mineral assemblages show no differential settling when a ramp is present, but differential settling occurred in a rimmed platform environment. This observation concurs with the palaeoenvironmental conditions of the Azazoul and Mohammed sections during the Cenomanian. Indeed, deposition in the Azazoul area occurred on a shallow ramp devoid of reef barriers to trap larger clay particles (Behrens *et al.*, 1978), whereas the Mohammed Beach section was deposited in the deeper Tarfaya Basin about 500 km to the south.

Sea-level variations over longer time periods during the Cretaceous were also postulated as a major cause for high smectite abundance at times of sea-level highstands and therefore due to differential settling of clay particles (Chamley *et al.*, 1990; Deconinck & Chamley, 1995; El Albani *et al.*, 1999). However, this correlation is not evident in Morocco (Chamley *et al.*, 1990; El Albani *et al.*, 1999). During the Cenomanian to early Turonian, smectite contents are constant and long-scale sea-level varies only slightly (Chamley *et al.*, 1990).

Based on these observations, clay mineral assemblages in shallow and deep depositional environments at Azazoul and Mohammed Beach are mostly the result of climate changes and can therefore be used as a climate proxy. However, caution is in order due to the slight differential settling overprint as a result of sea-level fluctuations.

At Azazoul Road, high kaolinite contents suggest a predominantly humid climate at the time of oyster limestone deposition during the early and middle Cenomanian. This long trend in humid

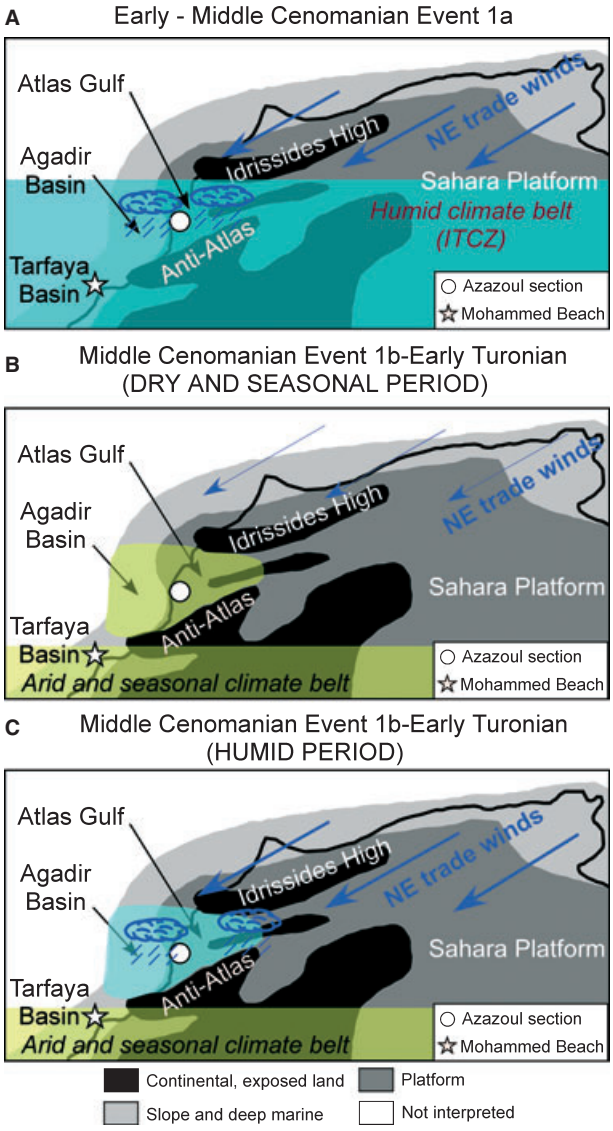

Fig. 16. Palaeoclimatic evolution from the early Cenomanian to early Turonian in the Agadir–Tarfaya area. A humid climate belt marks this area from early Cenomanian to MCE1a (A). A dry, seasonal climate belt moved southward by MCE1b, leading to dry and seasonally contrasted conditions in the Agadir–Tarfaya area (B). Intermittent humid periods are caused by stronger north-east trade winds bringing moisture from the Tethys and leading to high precipitation on the Atlas Gulf and Anti-Atlas (C).

conditions is interrupted by a period of high smectite indicative of dry and seasonal conditions (Fig. 12). During MCE1b, smectite increases and kaolinite decreases in a shale interval that indicates an abrupt climate change to drier and seasonal conditions (Fig. 12). During the middle to upper Cenomanian at Azazoul Beach, smectite predominates and is punctuated by short intervals of very high kaolinite contents (>90%) that suggest mostly dry seasonal conditions interrupted by short periods of pronounced humidity (Fig. 12). For example, high kaolinite contents indicative of very humid conditions prevailed during the first peak of the positive $\delta^{13}C$ characteristic of the OAE2 and are followed by a rapid change towards drier and more seasonal conditions (dominant smectite and the presence of palygorskyte; Fig. 12).

During the lower and middle Cenomanian at Mohammed Beach, high kaolinite contents indicate humid conditions up to MCE1a, correlative with humid conditions at Azazoul to the north. During the middle and upper Cenomanian, the gradual transition to high smectite contents indicates progressively drier and more seasonal conditions between MCE1a and MCE1b (Fig. 13). The relatively high IS mixed layer values in the OAE2 interval may be due to the high OM contents and alteration of smectite into IS mixed layers (Chamley, 1989) (Fig. 13).

Palaeoclimate of the Agadir–Tarfaya area

Palaeoclimate inferred from clay mineralogy in the Agadir–Tarfaya area is correlative during the lower and middle Cenomanian. Both sections indicate humid conditions up to MCE1b, followed by a drier seasonally contrasted climate (Fig. 16A). After MCE1b up to the lower Turonian, climate conditions decoupled between Azazoul and Mohammed Beach with variably humid conditions at Azazoul and a dry seasonal climate at Mohammed Beach (Fig. 16B and C). This decoupling is also observed in bulk rock mineralogy with relatively higher detrital input up to MCE1b at both locations (Figs 10 and 11). From MCE1b up to the lower Turonian, a gradual decrease in detrital input at Mohammed Beach is the result of a drier seasonally contrasted climate and a sea-level rise that led to carbonate-dominated sedimentation (Fig. 11). At Azazoul, detrital input is variable with high detrital influx during humid periods, except in oyster-dominated limestone beds (90% calcite). However, it is likely that terrigenous run-off continued or was even more important during the growth of oyster-dominated limestone beds, which depends on high nutrient influx derived largely from continental run-off (Pufahl & James, 2006; Gertsch *et al.*, 2010).

High variability in clay mineral assemblages and detrital indices at Azazoul is due mainly to its near-shore location (Fig. 1B) in the Agadir Gulf next to the Atlas chain (Behrens *et al.*, 1978; Wiedmann *et al.*, 1978). By contrast, Mohammed

Beach was situated in the Tarfaya Basin off the Morocco coast, where little or no relief was present (Wiedmann *et al.*, 1978). Azazoul clay mineral assemblages were influenced highly by climate variations due to changes in precipitation and increased continental run-off. The maximum decoupling is observed during OAE2 at Azazoul, as indicated by nearly 100% kaolinite. By contrast, no change is observed at Mohammed Beach, where kaolinite is absent.

Intertropical Convergence Zone and north-east trade wind variations during the Cenomanian

The differences in climate signals and the decoupling inferred from clay mineral assemblages at Azazoul and Mohammed Beach can be explained by variations in north-east trade wind intensity and latitudinal shifts of the Intertropical Convergence Zone (ITCZ) across western Africa. The ITCZ is defined as the dynamic boundary between south-east and north-east trade winds and is associated with a well-organized zonal band of low pressure and high precipitation that occurs predominantly over the ocean basin (Peterson & Haug, 2006). Today, the ICTZ extends over the Atlantic Ocean from South America to the west coast of Africa with latitudinal seasonal variations between 10°N and 20°N (July) and the equator (January). The largest latitudinal fluctuations occur on continents where the average position of the ITCZ lies at 6°N (Pettke *et al.*, 2002; Friedrich *et al.*, 2008).

Latitudinal position and variations are controlled mainly by eccentricity, precession, insolation and the percentage of continents per hemisphere. These factors influence the cross-equatorial gradient in sea surface temperatures, which trigger the distribution of sea-level pressure and winds (Nobre & Shukla, 1996; Chiang *et al.*, 2002). Over long periods (>1 Myr), changes in eccentricity (2·4 Myr cycle) will result in variations of latitudinal amplitude of the ITCZ. High eccentricity will cause high latitudinal variations of the ITCZ. Consequently, a large belt across the equator will be affected by the ITCZ over a year. The distribution of continents on Earth influences the mean position of the ITCZ, whereas precession acts on its short-term variations. Today, for example, the northern hemisphere contains 66% of the land on Earth (Floegel, 2001), which therefore triggers a mean position north of the equator (6°N).

During the Cenomanian to early Turonian the Azazoul–Tarfaya area was located at a palaeolatitude of *ca* 10°N (Philip, 2003; Skelton *et al.*, 2003; Floegel & Wagner, 2006). Ocean temperatures reached their maxima at the end of the Cenomanian and show a low equator to pole gradient (Pearson *et al.*, 2001; Huber *et al.*, 2002; Norris *et al.*, 2002). Continents were distributed evenly (Floegel, 2001). Based on these constraints, climate and ITCZ variations first modelled by Poulsen *et al.* (1999) suggest a mean latitudinal position at 7·5°S (Floegel & Wagner, 2006). However, the northern ITCZ boundary varies seasonally between 0°N and 15°N, whereas the southern boundary varies between 15°S and 0°S. Very high precipitation is postulated in tropical North Africa (Floegel & Wagner, 2006). Model results for the Cenomanian climate on land suggest tropical humid conditions between 0°N and 10°N in western Africa (Fluteau *et al.*, 2007), which concur with worldwide field - data summarized by Chumakov *et al.* (1995). Major problems with these models arise from the lack of climate variability and their rough estimates for periods spanning several million years.

At a similar palaeolatitude during the late Cenomanian to early Turonian in the Sinai, Egypt, Gertsch *et al.* (2010) recorded geochemical and climate records in sediments that are similar to Azazoul (for example, oyster biostromes, nodular marls and shales; Fig. 17). In the Sinai, humid conditions with high run-off and kaolinite input in the ocean prevailed during the late Cenomanian up to the first peak in $\delta^{13}C$ associated with OAE2; this is followed by drier and more seasonal conditions (smectite dominated and minor palygorskite) during the terminal Cenomanian and early Turonian.

Based on modelling and sedimentological data, the middle Cenomanian climate decoupling (end of MCE1b) appears to have been triggered by changes in eccentricity. At times of high eccentricity the ITCZ was positioned on the Agadir–Tarfaya area and therefore led to humid conditions. After MCE1b, lower eccentricity led to lower ITCZ amplitude variations and to seasonal and dry conditions over the Agadir–Tarfaya Basin. From MCE1b to the early Turonian, intermittent humid periods in Agadir are probably caused by stronger north-east trade winds, which brought moisture from the Tethys. The Anti-Atlas mountain range triggered abundant precipitations during periods of high north-east trade wind intensities. Therefore, very humid conditions occurred on the Atlas Gulf, whereas dry and seasonal conditions affected the Tarfaya Basin due to the rain shadow effect.

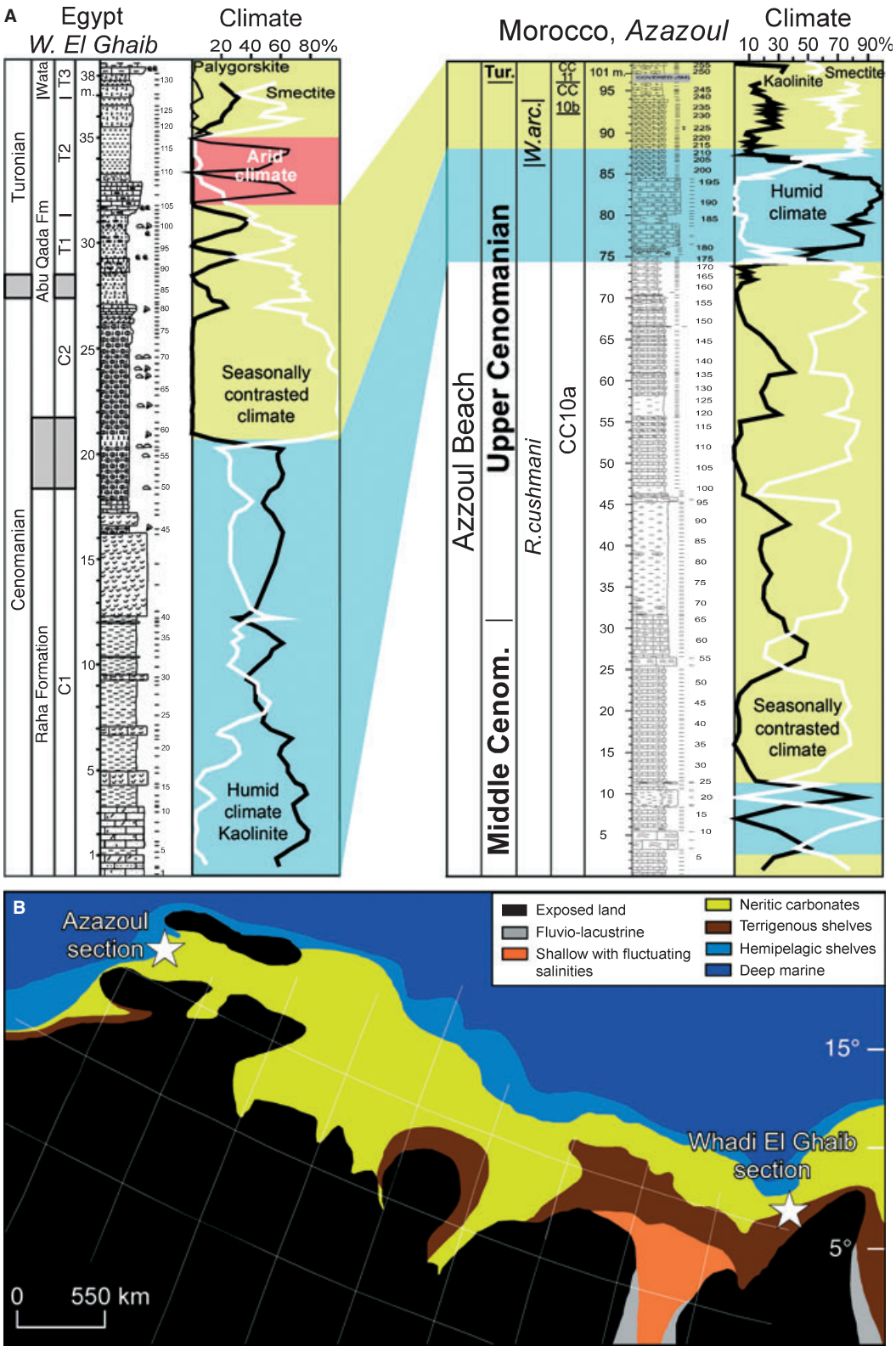

Fig. 17. (A) Palaeoclimate correlation for the late Cenomanian to early Turonian between Egypt (Gertsch *et al.*, 2010) and the Azazoul section of Morocco. Both sections reveal rapid climate change from humid to dry seasonally contrasted conditions near the end of the Cenomanian and into the early Turonian. (B) Palaeomap of the late Cenomanian with present-day latitudes and palaeolatitudes and palaeolongitudes during the late Cenomanian (white lines) (modified from Philip, 2003). Note that the Azazoul and Egypt sections are within the same palaeolatitude belt and experienced similar climate shifts.

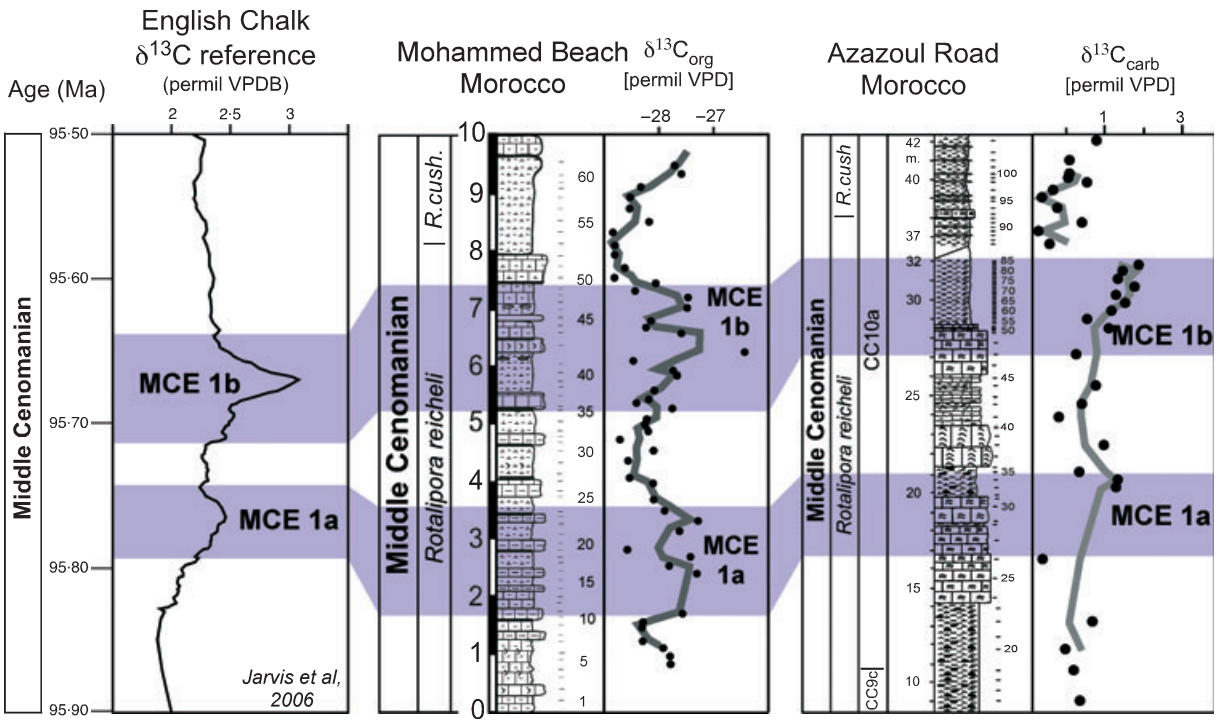

Fig. 18. $\delta^{13}C$ correlation between the two mid-Cenomanian events, MCE1a and MCE1b, of the English chalk composite curve (from Jarvis *et al.*, 2006), Mohammed Beach and Azazoul sections of Morocco (this study).

During OAE2, Floegel & Wagner (2006) suggest that an importation of humidity from south to north may have been the ultimate cause of black shale formation. This study also shows that climate change with high precipitation and run-off in tropical zones during the late Cenomanian was probably a major factor in black shale formation associated with the OAEs. At a global scale, this period of very humid conditions in the tropics during OAE2 correlates with the 'Plenus Cold Event' in the English Chalk (Pearce *et al.*, 2009). Kuhnt *et al.* (2009) suggest that eccentricity minima during periods of low variability in obliquity triggered a glacioeustatic lowstand prior to and at the onset of MCE and OAE2 events, but the glaciation hypothesis remains controversial as shown by new isotopic results from Blake Nose (Ando *et al.*, 2009). Therefore, global climate change induced by eccentricity cycles is probably an important factor for the OAE2 formation.

Mid-Cenomanian events

The middle Cenomanian events, MCE1a and MCE1b (MCE2 of Rodriguez-Lazaro *et al.*, 1998) are documented from sections in England, Italy, Spain and western USA where they occur in the lower part of the middle Cenomanian as two relatively closely spaced $\delta^{13}C$ excursions (Paul *et al.*, 1994; Rodriguez-Lazaro *et al.*, 1998; Coccioni & Galeotti, 2003; Jarvis *et al.*, 2006; Gale *et al.*, 2008). In the Dover section, England, carbon isotope values increased sharply by 0·5‰ to reach the first positive excursion at 2·3‰ (MCE1a), followed by a rapid fall to form a trough at 2·1‰ (Jarvis *et al.*, 2006). A 0·8‰ increase in $\delta^{13}C$ values to reach 2·9‰ corresponds to the second peak (MCE1b).

The two $\delta^{13}C$ excursions in the lower middle Cenomanian of the Azazoul and Mohammed Beach sections corroborate these observations. At Azazoul, oyster deposition prevents full characterization of MCE1a, although a 1‰ excursion is observed in the overlying shale (Fig. 18). MCE1b also follows oyster deposition, but the uppermost part of this excursion (*ca* 5 m) is covered by a landslide. At Mohammed Beach, MCE1a is marked by scattered high $\delta^{13}C_{org}$ values, whereas MCE1b marks a broad area of elevated values. The slight differences between the Mohammed Beach and Azazoul sections are probably due to diagenetic or preservation effects, and/or differences in the excursions of the $\delta^{13}C_{org}$ and $\delta^{13}C_{carb}$ data for the MCE events, respectively. In comparison with the $\delta^{13}C$ curve from the English Chalk (Jarvis *et al.*, 2006), the Azazoul MCE1a and MCE1b are about 1‰ lower. This difference may be due to the shallower deposi-

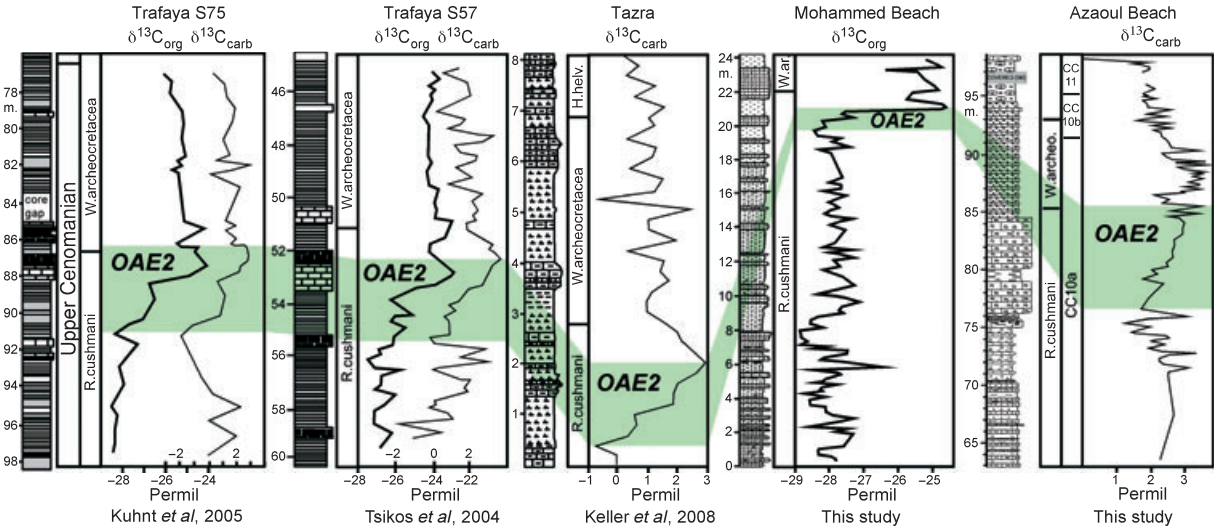

Fig. 19. $\delta^{13}C_{carb}$ and $\delta^{13}C_{org}$ correlation of late Cenomanian OAE2 excursion in the Tarfaya Basin (S75, S57, Tazra and Mohammed Beach) and Agadir Basin (Azazoul section).

tional environment at Azazoul (<50 m) when compared with the English Chalk (50 to 100 m).

Late Cenomanian OAE2

The late Cenomanian OAE2 carbon isotope record is well-known from deep-sea sections globally but relatively unknown from shallow-water environments. However, in the peri-Adriatic (Croatia), Portugal, Italy, Mexico and south-central Pyrenean (Spain) platforms the OAE2 $\delta^{13}C$ excursion was observed to be comparable with deep-water sections (Drzewiecky & Simo, 1997; Davey & Jenkyns, 1999; Parente *et al.*, 2007; Hart *et al.*, 2008; Elrick *et al.*, 2009). Recent studies in the Sinai observed the OAE2 excursion in shallow inner neritic environments where rare black shale deposition occurred (Gertsch *et al.*, 2010).

Regardless of the environment of deposition, the OAE2 $\delta^{13}C$ positive excursion shows characteristics similar to the global boundary stratotype section and point (GSSP) section at Pueblo (Keller *et al.*, 2004; Sageman *et al.*, 2006), including: (i) the rapid increase in carbon isotope values to the first peak; (ii) a short decrease of about 0·6‰ forming a trough; (iii) a rapid increase forming the second peak; and (iv) the prolonged plateau. These features are well-represented in the upper part of the Azazoul and Mohammed Beach sections (Fig. 8) and confirm the wide extent of the $\delta^{13}C$ signal.

Carbon and organic carbon isotope stratigraphy allows correlation of the Azazoul and Mohammed Beach sections with other coeval sedimentary successions globally. The magnitude of the OAE2 carbon excursion at Azazoul is comparable with the GSSP section at Pueblo, Colorado (about 2·2‰) but lower than at Eastbourne, England (Paul *et al.*, 1999; Jarvis *et al.*, 2006), and in Tarfaya [e.g. S75 (2·5‰), S57 (3·8‰) and Tazra (3‰), Fig. 19]. At Mohammed Beach, the OAE2 interval shows a similar $\delta^{13}C_{org}$ increase (4‰) as at Tarfaya (Fig. 19), but the presence of a condensed interval or hiatus is indicated by the sudden $\delta^{13}C$ shift.

Phosphorus concentrations and $\delta^{13}C$ trends show decreasing P concentrations during the gradual increase in $\delta^{13}C$ to the first peak of the OAE2 $\delta^{13}C$ excursion at Azazoul and Mohammed Beach (Fig. 15). The P concentrations remain low and reach their lowest values at the end of the $\delta^{13}C$ plateau. Similar P concentrations were observed previously by Mort *et al.* (2007, 2008), who also noticed a decoupling of the phosphorus and carbon cycles, supporting P regeneration and sustained productivity during OAE2. The latter is less evident at Azazoul, perhaps because of deposition in more oxic shallow water and oyster growth that does not record P concentrations in the same way as limestone or shale.

Delayed anoxia in shallow shelf environments

The faunal and floral turnovers of the middle and late Cenomanian have been described widely from shelf and deeper water sections, such as in Colorado (Keller & Pardo, 2004a; Keller *et al.*, 2004), England (Keller *et al.*, 2001), Italy (Luciani & Cobianchi, 1999; Mort *et al.*, 2007), Tunisia (Caron *et al.*, 2006) and the Tarfaya Basin of

Morocco (Kuhnt *et al.*, 1997; Kolonic *et al.*, 2005; Keller *et al.*, 2008). Although biotic changes in very shallow-water sections, such as Azazoul, are more difficult to quantify due to the sporadic occurrence of marine microfossils and rarity or absence of age diagnostic species, some environmental inferences can be drawn. A key feature of the shallow-water Azazoul sedimentary succession is the presence of oyster-rich limestone beds during the middle and late Cenomanian, which indicate shallow sub-tidal to estuarine environments and tolerate a wide range of environmental conditions (see *Sea-level* section above; Gertsch *et al.*, 2010).

Benthonic foraminiferal assemblages are rare in sub-tidal environments but increase in inner neritic settings. At Azazoul, benthonic abundance and diversity increases across and above the OAE2 $\delta^{13}C$ excursion, correlative with the sea-level rise and species assemblages, which consist mainly of abundant low oxygen-tolerant species (for example, *C. plaitum*, *G. sandidgei*, *N. albertensis* and *P. prolixa*, Figs 6 and 7); this suggests dysoxic bottom waters. By contrast, benthonic foraminifera in deeper marine environments are generally absent due to anoxic bottom waters (Keller *et al.*, 2001, 2004; Keller & Pardo, 2004a; Wagner *et al.*, 2004; Kuhnt *et al.*, 2005).

Planktonic foraminifera are rare in shallow shelf (sub-tidal and inner neritic) environments but allow correlation with the sea-level rise across the $\delta^{13}C$ excursion (Fig. 7). Assemblages are dominated by *H. planispira* and *H. delrioensis*, which are tolerant of reduced salinity in the shallow-water Pueblo section (Keller & Pardo, 2004b). Similarly, nannofossils *Broinsonia* spp. (*B. signata* and *B. matalosa*) are tolerant of reduced salinity (Roth & Krumbach, 1986; Bralower, 1988; Paul *et al.*, 1994, 1999). During the sea-level rise and $\delta^{13}C$ excursion more diverse assemblages appeared, including low oxygen-tolerant *Heterohelix* and *Whiteneinella* species (*W. archeocretacea* and *W. brittonensis*), suggesting a well-stratified ocean and high surface fertility; this is also indicated by the presence of common *Zeugrhabdotus* spp., an indicator for high surface water fertility (Roth & Krumbach, 1986; Shafik, 1990; Watkins *et al.*, 1996; Premoli Silva *et al.*, 1999; Lees, 2002). Dysoxic conditions prevailed into the lower Turonian laminated black shale interval, as indicated by *G. cenomana*, *Hedbergella* spp. and *Heterohelix* spp. (Jati, 2007).

Cenomanian sediments contain OM of both terrestrial and marine origin as a result of weak dysoxia in a marginal shelf setting and high continental run-off during humid periods. Rock-Eval data also suggest that some of the marine-sourced OM is altered. During the lower Turonian, increasingly laminated sediments with marine OM (Jati, 2007) mark the onset of anoxic conditions as sea-level rises to middle neritic depths.

Organic matter preservation, shallow-water planktonic and benthonic foraminifera and nannofossil assemblages indicate dysoxic, brackish and mesotrophic conditions during the OAE2 at Azazoul. Anoxic marine conditions were not reached until the lower Turonian, suggesting a delay in anoxia in these shallow marginal environments, as also observed by lower Turonian altered laminated shale in the Sinai (Gertsch *et al.*, 2010) and in the Western Interior Sea (Leckie *et al.*, 1998). By contrast, OAE2 is associated with anoxic conditions and better organic carbon preservation in outer shelf and deeper basin environments like Mohammed Beach in the Tarfaya Basin.

CONCLUSIONS

- Middle Cenomanian events 1a and 1b (MCE1a and MCE1b) and late Cenomanian oceanic anoxic event 2 (OAE2) in the Agadir–Tarfaya area of Morocco are recorded globally in $\delta^{13}C$ excursions from inner neritic (Agadir and Azazoul) to open marine environments (Tarfaya).
- Sub-tidal to inner neritic environments during MCE and OAE2 events (at Azazoul) are characterized by dysoxic, brackish and mesotrophic conditions, as indicated by planktonic and benthonic foraminifera, nannofossil and macrofossil (for example, oysters) assemblages.
- Anoxic bottom conditions (laminated black shale deposition) are restricted to deeper waters (middle neritic and deeper) associated with the maximum sea-level rise during the early Turonian (Azazoul). In contrast to the latest Cenomanian anoxia in deeper environments, this indicates a delay in shallow-water sequences until a critical water depth is reached.
- Sea-level changes inferred from lithology, microfossils and macrofossils at Azazoul reveal low-amplitude short-term sea-level falls superimposed on the major well-known sea-level variations.
- Palaeoclimate evolution of the Agadir–Tarfaya area reveals climate decoupling in the middle Cenomanian (after MCE1b), which appears to be related to the southward shift of

the Intertropical Convergence Zone that was triggered probably by changes in eccentricity. This effect is indicated by constant dry seasonal conditions in the Tarfaya Basin, and alternating humid and dry seasonal conditions at Agadir, probably as a result of short-term changes in north-east trade wind intensity and moisture input from the Tethys.

- Humid conditions prevailed at Agadir during the onset of OAE2, followed by drier and more seasonal conditions. Similar climate trends were observed in similar palaeoenvironments at the same palaeolatitude in Egypt (Gertsch *et al.*, 2010), which suggests that climate change was a critical factor in the formation of OAE2 and black shale deposition.

ACKNOWLEDGEMENTS

We thank the reviewers M. Leckie, W. Kuhnt and one anonymous, for comments and helpful suggestions. We also thank Adam Maloof for insightful discussions and H. Chellai, Marrakech University for help on the field. This research was supported by NSF International Programs grant INT-0115357 (GK) and the Swiss National Foundation FNS grant 200020-119943/1 (TA).

REFERENCES

Adatte, T. and **Rumley, G.** (1989) Sedimentology and mineralogy of Valanginian and Hauterivian in the stratotypic region (Jura mountains, Switzerland). In: *Cretaceous of the Western Tethys Proceedings of the Third International Cretaceous Symposium, Tübingen, 1987* (Ed. J. Wiedmann), pp. 329–351. Ed Scheizerbart'sche verlagsbuchandlhung, Stuttgart.

Adatte, T., Stinnesbeck, W. and **Keller, G.** (1996) Lithostratigraphic and mineralogic correlations of near K/T boundary sediments northeastern Mexico: implications for origin and nature of deposition. In: *The Cretaceous-Tertiary Event and Other Catastrophes in Earth History, Boulder, Colorado* (Eds G. Ryder, D. Fastovsky and S. Gartner), *Geol. Soc. Am. Spec. Pap.*, **307,** 211–226.

Adatte, T., Keller, G. and **Stinnesbeck, W.** (2002) Late Cretaceous to early Paleocene climate and sea-level fluctuations: the Tunisian record. *Palaeogeogr. Palaeoclimatol. Palaeoecol.*, **178,** 165–196.

Ando, A., Huber, B.T., MacLeod, K.G., Ohta, T. and **Khim, B.-K.** (2009) Blake Nose stable isotopic evidence against the mid-Cenomanian glaciation hypothesis. *Geology*, **37,** 451–454.

Andreu, B. (1989) Le Cretace moyen de la transversale Agadir–Nador (Maroc): precisions stratigraphiques et sedimentologiques. *Cretaceous Res.*, **10,** 49–80. DOI: 10.1016/0195-6671(89)90029-3.

Arthur, M.A. and **Sageman, B.B.** (1994) Marine black shales: depositional mechanisms and environments of ancient deposits. *Annu. Rev. Earth Planet. Sci.* **22,** 499–551.

Arthur, M.A., Dean, W.E. and **Pratt, L.M.** (1988) Geochemical and climatic effects of increased marine organic-carbon burial at the Cenomanian–Turonian boundary. *Nature*, **335,** 714–717.

Bauer, J., Marzouk, A.M., Steuber, T. and **Kuss, J.** (2001) Lithostratigraphy and biostratigraphy of the Cenomanian–Santonian strata of Sinai, Egypt. *Cretaceous Res.*, **22,** 497–526.

Behar, F., Beaumont, V. and **De B. Penteado, H.L.** (2001) Rock-Eval 6 technology: performances and developments. *Oil Gas Sci. Technol.*, **56,** 111–134.

Behrens, M., Krumsiek, K., Meyer, D.E., Schafer, A., Siehl, A., Stets, J., Thein, J. and **Wurster, P.** (1978) Sedimentationsablaufe im Atlas-Golf (Kreide Kustenbelcken Marokko). *Geol. Rundsch.*, **67,** 424–453.

Bodin, S., Godet, A., Follmi, K.B., Vermeulen, J., Arnaud, H., Strasser, A., Fiet, N. and **Adatte, T.** (2006) The late Hauterivian Faraoni ocenic event in the western Tethys: evidence from phosphorus burial rates. *Paleogeogr. Palaeoclimatol. Palaeoecol.*, **235,** 245–264.

Bolli, H.M., Beckmann, J.-P. and **Sauders, J.B.** (1994) *Benthic Foraminiferal Biostratigraphy of the South Caribbean Region*. Cambridge University press, Cambridge, 408 pp.

Bralower, T.J. (1988) Calcareous nannofossil biostratigraphy and assemblages of the Cenomanian–Turonian boundary interval: implications for the origin and timing of oceanic anoxia. *Palaeoceanography*, **3,** 275–316.

Bralower, T.J., Leckie, R.M., Sliter, W.V. and **Thierstein, H.R.** (1995) An integrated Cretaceous microfossil biostratigraphy. In: *Geochronology Time Scales and Global Stratigraphic Correlation* (Eds W.A. Berggren, D.V. Kent, M.P. Aubry and J. Hardenbol), *SEPM Spec. Publ.*, **54,** 56–79.

Buonocunto, F.P., Sprovieri, M., Bellanca, A., D'Argenio, B., Ferreri, V., Neri, R. and **Ferruzza, G.** (2002) Cyclostratigraphy and high-frequency carbon isotope fluctuations in Upper Cretaceous shallow-water carbonates, southern Italy. *Sedimentology*, **49,** 1321–1337.

Burnett, J.A. (1996) Nannofossils and Upper Cretaceous (sub-) stage boundaries – state of the art. *Journal of Nannoplankton Research*,**18,** 23–32.

Burnett, J.A. (1998) Upper Cretaceous. In: *Calcareous Nannofossil Biostratigraphy* (Ed. P.R. Bown), pp. 132–199. Chapman & Hall, London.

Canfield, D.E. (1994) Factors influencing organic carbon preservation in marine sediments. *Chem. Geol.*, **114,** 315–329.

Caron, M. (1985) Cretaceous planktonic foraminifera. In: *Plankton Stratigraphy* (Eds H.M. Bolli, J.B. Saunders and K. Perch-Nielsen), pp. 17–86. Cambridge University Press, Cambridge.

Caron, M., Dall'Agnolo, S., Accarie, H., Barrera, E., Kauffman, E.G., Amedro, F. and **Robaszynski, F.** (2006) High-resolution stratigraphy of the Cenomanian–Turonian boundary interval at Pueblo (USA) and wadi Bahloul (Tunisia) stable isotope and bio-events correlation. *Geobios*, **39,** 171–200.

Chamley, H. (1989) *Clay Sedimentology*. Springer Verlag, Berlin, 623 pp.

Chamley, H., Deconinck, J.-F. and **Millot, G.** (1990) Sur l'abondance des mineraux smectitiques dans les sediments marins communs deposes lors des periodes de haut niveau marin du Jurassique superieur au Paleogene. *CR Acad. Sci. Paris*, **t. 311, Serie II,** 1529–1536.

Chiang, J.C.H., Kushnir, Y. and **Giannini, A.** (2002) Deconstructing Atlantic Intertropical Convergence Zone variability: influence of the local cross-equatorial sea surface temperature gradient and remote forcing from the eastern equatorial Pacific. *J. Geophys. Res.*, **107,** 4004.

Chumakov, N.M., Zharkov, M.A., Herman, A.B., Doludenko, M.P., Kalandadze, N.N., Lebedev, E.L., Ponomarenko, A.G. and **Raurian, A.S.** (1995) Climatic belts of the Mid-Cretaceous time. *Stratigr. Geol. Correlation*, **3,** 241–260.

Clarke, L.J. and **Jenkyns, H.C.** (1999) New oxygen isotope evidence for long-term Cretaceous climatic change in the Southern Hemisphere. *Geology*, **27,** 699–702.

Coccioni, R. and **Galeotti, S.** (2003) The mid-Cenomanian Event: prelude to OAE2. *Paleogeogr. Palaeoclimatol. Palaeoecol.*, **190,** 427–443.

Courtillot, V.E. and **Renne, P.R.** (2003) On the ages of flood basalt events. *CR Geosci.* **335,** 113–140.

Davey, S.D. and **Jenkyns, H.C.** (1999) Carbon-isotope stratigraphy of shallow-water limestones and implications for the timing of Late Cretaceous sea-level rise and anoxic events (Cenomanian–Turonian of the peri-Adriatic carbonate platform, Croatia). *Eclogae Geol. Helv.*, **92,** 163–170.

Deconinck, J.-F. and **Chamley, H.** (1995) Diversity of smectite origins in late Cretaceous sediments: example of chalks from northern France. *Clay Mineral.*, **30,** 365–379.

Dhondt, A.V., Malchus, N., Boumaza, L. and **Jaillard, E.** (1999) Cretaceous oysters from North Africa: origin and distribution. *Bull. Soc. Geol. Fr.*, **170,** 67–76.

Drzewiecky, P.A. and **Simo, J.A.** (1997) Carbonate platform frowning and oceanic anoxic events on a mid-Cretaceous carbonate platform, south-central Pyrenees, Spain. *J. Sed. Res.*, **67,** 698–714.

El Albani, A., Kuhnt, W., Luderer, F., Herbin, J.P. and **Caron, M.** (1999) Palaeoenvironmental evolution of the Late Cretaceous sequence in the Tarfaya Basin (southwest of Morocco). In: *The Oil and Gas Habitats of the South Atlantic* (Eds N.R. Cameron, R.H. Bate and V.S. Clure), *Geol. Soc. London Spec. Publ.*, **153,** 223–240.

Elrick, M., Molina-Garza, R., Duncan, R. and **Snow, L.** (2009) C-isotope stratigraphy and paleoenvironmental changes across OAE2 (mid-Cretaceous) from shallow-water platform carbonates of southern Mexico. *Earth Planet. Sci. Lett.*, **277,** 295–306.

Erba, E. and **Tremolada, F.** (2004) Nannofossil carbonate fluxes during the Early Cretaceous: phytoplankton response to nutrification episodes, atmospheric CO_2, and anoxia. *Paleoceanography* **19,** Article No. PA 1008.

Erbacher, J., Thurow, J. and **Littke, R.** (1996) Evolution patterns of radiolaria and organic matter variations: a new approach to identify sea-level changes in mid-Cretaceous pelagic environments. *Geology*, **24,** 499–502.

Espitalié, J., Deroo, G. and **Marquis, F.** (1985) La pyrolyse Rock-Eval et ses applications. *Rev. Inst. Fr. Pétrol.*, **40,** 563–579.

Floegel, S. (2001) *On the influence of precessional milankovitch cycles on the late Cretaceous climate system: comparison of GCM-results, geochemical and sedimentary proxies for the western interior seaway of north America*. Doctoral Thesis, Kiel University, 236 pp.

Floegel, S. and **Wagner, T.** (2006) Insolation-control on the Late Cretaceous hydrological cycle and tropical African climate-global climate modeling linked to marine climate records. *Paleogeogr. Palaeoclimatol. Palaeoecol.*, **235,** 288–304.

Fluteau, F., Ramstein, G., Besse, J., Guiraud, R. and **Masse, J.P.** (2007) Impacts of paleogeography and sea level changes on Mid-Cretaceous climate. *Paleogeogr. Palaeoclimatol. Palaeoecol.*, **247,** 357–381.

Forster, A., Schouten, S., Moriya, K., Wilson, P.A. and **Sinninghe Damste, J.S.** (2007) Tropical warming and intermittent cooling during the Cenomanian/Turonian oceanic anoxic event 2: sea surface temperature records from the equatorial Atlantic. *Paleoceanography*, **22,** PA1219. DOI: 10.1029/2006PA001349.

Friedrich, O., Norris, R.D., Bornemann, A., Beckmann, B., Palike, H., Worstell, P., Hofmann, P. and **Wagner, T.** (2008) Cyclic changes in Turonian to Coniacian planktic foraminiferal assemblages from the tropical Atlantic Ocean. *Mar. Micropaleontol.*, **68,** 299–313.

Gale, A.S., Smith, A.B., Monks, N.E.A., Young, J.A., Howard, A., Wray, D.S. and **Huggett, J.M.** (2000) Marine biodiversity through the Late Cenomanian–Early Turonian: palaeoceanographic controls an d sequence stratigraphic biases. *J. Geol. Soc.*, **157,** 745–757.

Gale, A.S., Hardenbol, J., Hathway, B., Kennedy, W.J., Young, J.R. and **Phansalkar, V.** (2002) Global correlation of Cenomanian (Upper Cretaceous) sequences: evidence for Milankovitch control on sea level. *Geology*, **30,** 291–294.

Gale, A.S., Voigt, S., Sageman, B.B. and **Kennedy, W.J.** (2008) Eustatic sea-level record for the Cenomanian (Late Cretaceous) – extension to the Western Interior Basin, USA. *Geology*, **36,** 859–862.

Gertsch, B., Adatte, T., Keller, G., Berner, Z., Stueben, D., Tantawy, A.A.A.M. and **Mort, H.P.** (2010) Cenomanian–Turonian transition in shallow water sequences of the Sinai, Egypt. *Int. J. Earth Sci. (Geol. Rundsch.)*, **99,** 165–182.

Glenn, C.R. and **Arthur, M.A.** (1990) Anatomy and origin of a Cretaceous phosphorite-green sand giant, Egypt. *Sedimentology*, **37,** 123–148.

Godet, A., Bodin, S., Adatte, T. and **Foellmi, K.B.** (2008) Clay mineral assemblages along the Northern Tethyan margin during the Late Hauterivian–Early Aptian: interactions between climate change and carbonate platform evolution. *Cretaceous Res.*, **29,** 830–847.

Grotsch, J., Billing, I. and **Vahrenkamp, V.** (1998) Carbon-isotope stratigraphy in shallow-water carbonates: implications for Cretaceous black-shale deposition. *Sedimentology*, **45,** 623–634.

Gustafsson, M., Holbourn, A. and **Kuhnt, W.** (2003) Changes in Northeast Atlantic temperature and carbon flux during the Cenomanian/Turonian paleoceanographic event: the Goban Spur stable isotope record. *Palaeogeogr. Palaeoclimatol. Palaeoecol.*, **201,** 51–66.

Hallam, A. (1992) *Phanerozoic Sea Level Changes*. Columbia Press, New York.

Haq, B.U., Hardenbol, J. and **Vail, P.R.** (1987) Chronology of fluctuating sea levels since the Triassic. *Science*, **235,** 1156–1167.

Hardenbol, J., Thierry, J., Farley, M.B., de Graciansky, P.C. and **Vail, P.P.** (1998) Mesozoic and Cenozoic sequence chronostratigraphic framework of European basins. In: *Mesozoic and Cenozoic Sequence Stratigraphy of European Basins* (Eds P.C. de Graciansky, J. Hardenbol, T. Jacquin and P.P. Vail), *Soc. Sed. Geol. Spec. Publ.*, **60,** 3–13.

Hart, M.B. and **Leary, P.N.** (1989) The stratigraphic and paleogeographic setting of the late Cenomanian anoxic event. *J. Geol. Soc.*, **146,** 305–310.

Hart, M.B., Callapez, P.M., Fisher, J.K., Hannant, K., Monteiro, J.F., Price, G.D. and **Watkinson, M.P.** (2008) Micro-

paleontology and stratigraphy of the Cenomanian/Turonian boundary in the Lusitanian Basin, Portugal. *J. Iberian Geol.*, **31,** 311–326.

Huber, B.T., Hodell, D.A. and **Hamilton, C.P.** (1995) Middle–Late Cretaceous climate of the southern high-latitudes – stable isotopic evidence for minimal equator-to-pole thermal-gradients. *Geol. Soc. Am. Bull.*, **107,** 1164–1191.

Huber, B.T., Norris, R.D. and **MacLeod, K.G.** (2002) Deep-sea paleotemperature record of extreme warmth during the Cretaceous. *Geology*, **30,** 123–126.

Jarvis, I., Gales, A.S., Jenkyns, H.C. and **Pearce, M.A.** (2006) Secular variation in Late Cretaceous carbono isotopes: a new $\delta^{13}C$ carbonate reference curve for the Cenomanian–Campanian (99.6–70.6 Ma). *Geol. Mag.*, **143,** 561–608.

Jati, M. (2007) Le passage Cénomanien–Turonien du continent nord africain (Maroc, Algérie, Tunisie). Comparaison avec le bassin subalpin: apport de la sédimentologie et de la géochimie isotopique. Université Louis Pasteur, Ecole et observatoire des Sciences de la Terre, UMR 7517 du CNRS, Strasbourg, 247 pp.

Jenkyns, H.C. (1980) Cretaceous anoxic events – from continents to oceans. *J. Geol. Soc.*, **137,** 171–188.

Jenkyns, H.C. (1991) Impact of Cretaceous sea level rise and anoxic events on the Mesozoic carbonate platform of Yugoslavia. *AAPG Bull.*, **75,** 1007–1017.

Jenkyns, H.C., Gale, A.S. and **Corfield, R.M.** (1994) Carbon- and oxygen-isotope stratigraphy of the English Chalk and Italian Scaglia and its palaeoclimatic significance. *Geol. Mag.*, **131,** 1–34.

Keller, G. and **Pardo, A.** (2004a) Age and paleoenvironment of the Cenomanian–Turonian global stratotype section and point at Pueblo, Colorado. *Mar. Micropaleontol.*, **51,** 95–128.

Keller, G. and **Pardo, A.** (2004b) Disaster opportunists Guembelitrinidae: index for environmental catastrophes. *Mar. Micropaleontol.*, **53,** 83–116.

Keller, G., Li, L. and **MacLeod, N.** (1995) The Cretaceous/Tertiary boundary stratotype section at El Kef, Tunisia: how catastrophic was the mass extinction? *Paleogeogr. Palaeoclimatol. Palaeoecol.*, **119,** 221–254.

Keller, G., Han, Q., Adatte, T. and **Burns, S.J.** (2001) Palaeoenvironment of the Cenomanian–Turonian transition at Eastbourne, England. *Cretaceous Res.*, **22,** 391–422.

Keller, G., Berner, Z., Adatte, T. and **Stueben, D.** (2004) Cenomanian–Turonian and delta C-13, and delta O-18, sea level and salinity variations at Pueblo, Colorado. *Palaeogeogr. Palaeoclimatol. Palaeoecol.*, **211,** 19–43.

Keller, G., Tantawy, A.A., Berner, Z., Adatte, T., Chellai, E.H. and **Stueben, D.** (2008) Oceanic events and biotic effects of the Cenomanian–Turonian anoxic event, Tarfaya Basin, Morocco. *Cretaceous Res.*, **29,** 976–994.

Kennedy, W.J., Gale, A.S., Lees, J.A. and **Caron, M.** (2006) The global boundary stratotype section and point (GSSP) for the base of the Cenomanian Stage, Mont Risou, Hautes-Alpes, France. *Episodes*, **27,** 21–30.

Kerr, A.C. (1998) Oceanic plateau formation: a cause of mass extinction and black shale deposition around the Cenomanian–Turonian boundary? *J. Geol. Soc. London*, **155,** 619–626.

Kolonic, S., Wagner, T., Forster, A., Sinninghe Damste, J.S., Walsworth-Bell, B., Erba, E., Turgeon, S., Brumsack, H.J., Chellai, E.H., Tsikos, H., Kuhnt, W. and **Kuypers, M.M.M.** (2005) Black shale deposition on the northwest African Shelf during the Cenomanian/Turonian oceanic anoxic event: climate coupling and global organic carbon burial. *Paleoceanography* **20,** Article No. PA1006.

Kübler, B. (1983) Dosage quantitatif des minéraux majeurs des roches sédimentaires par diffraction X. *Cah. Inst. Geol.*, **Series AX no. 1.1 and 1.2,** 1–13.

Kübler, B. (1987) Cristallinité de l'illite: méthode normalisées de préparation de mesure, méthode automatique normalisées de mesure. *Cah. Inst. Geol.*, Suisse Serie ADX number 2.

Kübler, B. and **Jaboyedoff, M.** (2000) Illite cristallinity. *CR Acad. Sci. Paris/Earth Planet. Sci.*, **331,** 75–89.

Kuhnt, W., Nederbragt, A. and **Leine, L.** (1997) Cyclicity of Cenomanian–Turonian organic-carbon-rich sediments in the Tarfaya Atlantic Coastal Basin (Morocco). *Cretaceous Res.* **18,** 587–601.

Kuhnt, W., Luderer, F., Nederbragt, S., Thurow, J. and **Wagner, T.** (2005) Orbital-scale record of the late Cenomanian–Turonian oceanic anoxic event (OAE-2) in the Tarfaya Basin (Morocco). *Int. J. Earth Sci. (Geol. Rundsch.)*, **94,** 147–159.

Kuhnt, W., Holbourn, A., Gale, A., Chellai, E.H. and **Kennedy, W.J.** (2009) Cenomanian sequence stratigraphy and sea-level fluctuations in the Tarfaya Basin (SW Morocco). *GSA Bull.*, **121,** 1695–1710.

Kuypers, M.M.M., Pancost, R.D., Nijenhuis, I.A. and **Sinninghe Damste, J.S.** (2002) Enhanced productivity led to increased organic carbon burial in the euxinic North Atlantic basin during the late Cenomanian oceanic anoxic event. *Paleoceanography* **17,** Article No. PA1051.

Larson, R.L. (1991) Latest pulse of earth – evidence for a mid Cretaceous superplume. *Geology*, **19,** 547–550.

Larson, R.L. and **Erba, E.** (1999) Onset of the mid-Cretaceous greenhouse in the Barremian–Aptian: igneous events and the biological, sedimentary, and geochemical responses. *Paleoceanography*, **14,** 663–678.

Leckie, R.M., Yurevitch, R.M., West, O.L., Finkelstein, D. and **Schmid, M.G.** (1998) Paleoceanography of the southwestern Western Interior sea during the time of the Cenomanian–Turonian boundary (Late Cretaceous). In: *Stratigraphy and Paleoenvironments of the Cretaceous Interior Seaway, USA* (Eds W.E. Dean and M.A. Arthur), *SEPM Concepts Sedimentol. Paleontol.*, **6,** 101–126.

Leckie, R.M., Bralower, T.J. and **Cashman, R.** (2002) Oceanic anoxic events and plankton evolution: biotic response to tectonic forcing during the mid-Cretaceous. *Paleoceanography* **17,** 13.1–13.29.

Lees, J.A. (2002) Calcareous nannofossil biostratigraphy illustrates palaeoclimate change in the Late Cretaceous Indian Ocean. *Cretaceous Res.*, **23,** 537–634.

Luciani, V. and **Cobianchi, M.** (1999) The Bonarelli level and other black shales in the Cenomanian–Turonian of the northeastern Dolomites (Italy): calcareous nannofossil and foraminiferal data. *Cretaceous Res.*, **20,** 135–167.

Luning, S., Kolonic, S., Belhadj, E.M., Cota, L., Baric, G. and **Wagner, T.** (2004) Integrated depositional model for the Cenomanian–Turonian organic-rich strata in North Africa. *Earth-Sci. Rev.*, **64,** 51–117.

Marshall, J.D. (1992) Climatic and oceanographic isotopic signals from the carbonate rock record and their preservation. *Geol. Mag.*, **129,** 143–160.

Mort, H.P., Adatte, T., Foellmi, K.B., Keller, G., Steinmann, P., Matera, V., Berner, Z. and **Stueben, D.** (2007) Phosphorus and the roles of productivity and nutrient recycling during Oceanic Event 2. *Geology*, **35,** 483–486.

Mort, H.P., Adatte, T., Keller, G., Bartels, D., Follmi, K.B., Steinmann, P., Berner, Z. and **Chellai, E.H.** (2008) Organic

carbon deposition and phosphorus accumulation during Oceanic Anoxic Event 2 in Tarfaya, Morocco. *Cretaceous Res.* **29,** 1008–1023.

Müller, R., Sdrolias, M., Gaina, C., Steinberger, B. and **Heine, C.** (2008) Long-term sea-level fluctuations driven by ocean basin dynamics. *Nature*, **319,** 1357–1362.

Nobre, P. and **Shukla, J.** (1996) Variations of sea temperature, wind stress and rainfall over the tropical Atlantic and South America. *J. Clim.*, **9,** 2464–2479.

Norris, R.D., Bice, K.L., Magno, E.A. and **Wilson, P.A.** (2002) Jiggling the tropical thermostat in the Cretaceous hothouse. *Geology*, **30,** 299–302.

Pardo, A., Adatte, T., Keller, G. and **Oberhansli, H.** (1999) Paleoenvironmental changes across the Cretaceous–Tertiary boundary at Koshak, Kazakhstan, based on planktic foraminifera and clay mineralogy. *Paleogeogr. Palaeoclimatol. Palaeoecol.* **154,** 247–273.

Parente, M., Frijia, G. and **Di Lucia, M.** (2007) Carbon-isotope stratigraphy of Cenomanian–Turnonian platform carbonates from the southern Apennines (Italy): a chemostratigraphy approach to the problem of correlation between shallow-water and deep-water successions. *J. Geol. Soc.*, **164,** 609–620.

Paul, C.R.C., Mitchell, S.F., Lamolda, M.A. and **Gorostidi, A.** (1994) The Cenomanian–Turonian boundary event in northern Spain. *Geol. Mag.*, **131,** 801–817.

Paul, C.R.C., Lamolda, M.A., Mitchell, S.F., Vaziri, M.R., Gorostidi, A. and **Marshall, J.D.** (1999). The Cenomanian–Turonian boundary at Eastbourne (Sussex, UK): a proposed European reference section. *Paleogeogr. Palaeoclimatol. Palaeoecol.*, **150,** 83–121.

Pearce, M.A., Jarvis, I. and **Tocher, B.A.** (2009) The Cenomanian–Turonian boundary event, OAE2 and palaeoenvironmental change in epicontinental seas: new insights from the dinocyst and geochemical records. *Palaeogeogr. Palaeoclimatol. Palaeoecol.*, **280,** 207–234.

Pearson, P.N., Ditchfield, P.W., Singano, J., Harcourt-Brown, K.G., Nicholas, C.J., Olsson, R.K., Shackleton, N.J. and **Hall, M.A.** (2001) Warm tropical sea surface temperatures in the Late Cretaceous and Eocene epochs. *Nature*, **413,** 481–487.

Pedersen, T.F. and **Calvert, S.E.** (1990) Anoxia vs Productivity – what controls the formation of organic-carbon-rich sediments and sedimentary rocks. *AAPG Bull.*, **74,** 454–466.

Perch-Nielsen, K. (1985) Cenozoic calcareous nannofossils. In: *Plankton Stratigraphy* (Eds H.M. Bolli, J.B. Saunders and K. Perch-Nielsen), pp. 422–454. Cambridge University Press, Cambridge.

Peterson, L.C. and **Haug, G.H.** (2006) Variability in the mean latitude of the Atlantic Intertropical Convergence Zone as recorded by riverine input of sediments to the Cariaco Basin (Venezuela). *Paleogeogr. Palaeoclimatol. Palaeoecol.*, **234,** 97–113.

Pettke, T., Halliday, A.N. and **Rea, D.K.** (2002) Cenozoic evolution of Asian climate and sources of Pacific seawater Pb and Nd derived from eolian dust of sediment core LL44-GPC3. *Paleoceanography*, **17,** 3. DOI: 10.1029/2001PA000673.

Philip, J. (2003) Peri-Tethyan neritic carbonate areas: distribution through time and driving factors. *Palaeogeogr. Palaeoclimatol. Palaeoecol.*, **196,** 19–37.

Poulsen, C.J., Barron, E.J., Johnson, C.C. and **Fawcett, P.** (1999). Links between major climatic factors and regional oceanic circulation in the Mid-Cretaceous. In: *Evolution of the Cretaceous Ocean Climate System* (Eds E. Barrera and C.C. Johnson), Geol. Soc. Am. Spec. Pap., 73–89.

Pratt, L.M., Arthur, M.A., Dean, W.E. and **Scholle, P.A.** (1993) Paleoceanographic cycles and events during the late Cretaceous in the Western Interior Seaway of North America. In: *Evolution of the Western Interior Basin, St. John's* (Eds W.G. E Caldwell and E.G. Kauffman), *Geol. Assoc. Canada Spec. Pap.*, **39,** 333–354.

Premoli Silva, I., Erba, E., Salvini, G., Verga, D. and **Locatelli, C.** (1999) Biotic changes in Cretaceous anoxic events. *J. Foram. Res.*, **29,** 352–370.

Pufahl, P.K. and **James, N.P.** (2006) Monospecific Pliocene oyster buildups, Murray Basin, South Australia: brackish water end member of the reef spectrum. *Paleogeogr. Palaeoclimatol. Palaeoecol.*, **233,** 11–33.

Robaszynski, F. and **Caron, M.** (1979) Atlas de foraminiferes planctoniques du Cretace moyen (Mer boreale et Tethys), premiere partie. *Cah. Micropaleontol.* **1,** 185.

Robaszynski, F., Caron, M., Dupuis, C., Amédro, F., Gonzalez Donoso, J.M., Linares, D., Hardenbol, J., Gartner, S., Calandra, F. and **Deloffre, R.** (1990) A tentative integrated stratigraphy in the Turonian of central Tunisia: formations, zones and sequential stratigraphy in the Kalaat Senan area. *Bull. Centres Rech. Explor.-Prod. Elf Aquitaine*, **14,** 213–384.

Rodriguez-Lazaro, J., Pascual, A. and **Elorza, J.** (1998) Cenomanian events in the deep western Basque Basin: the Leioa section. *Cretaceous Res.*, **19,** 673–700.

Roth, P.H. and **Krumbach, K.R.** (1986) Middle Cretaceous calcareous nannofossil biogeography and preservation in the Atlantic and Indian oceans: implications for palaeoceanography. *Mar. Micropaleontol.*, **10,** 235–266.

Sageman, B.B., Rich, J., Arthur, M.A., Dean, W.E., Savrda, C.E. and **Bralower, T.J.** (1998) Multiple Milankovitch cycles in the Bridge Creek Limestone (Cenomanian–Turonian), Western Interior Basin. In: *Concepts in Sedimentology and Paleontology*, Vol. 6, pp. 153–171. SEPM, Tulsa, OK.

Sageman, B.B., Meyers, S.R. and **Arthur, M.A.** (2006) Orbital timescale and new C-isotope record for Cenomanian–Turonian boundary stratotype. *Geology*, **34,** 125–128.

Sahagian, D., Pinous, O., Olferiev, A. and **Zakharov, V.** (1996) Eustatic curve for the Middle Jurassic–Cretaceous based on Russian Platform and Siberian stratigraphy: zonal resolution. *AAPG Bull.*, **80,** 1433–1458.

Schlanger, S.O., Arthur, M.A., Jenkyns, H.C. and **Scholle, P.A.** (1987) The Cenomanian–Turonian oceanic anoxic event, I. Stratigraphy and distribution of organic carbon-rich beds and the marine $\delta^{13}C$ excursion. In: *Marine Petroleum Soucre Rocks* (Eds J. Brooks and A.J. Fleet), *Spec. Publ. Geol. Soc. Lond.*, **26,** 371–399.

Schrag, D.P., DePaolo, D.J. and **Richter, F.M.** (1995) Reconstructing past sea surface temperatures: correcting for diagenesis of bulk marine carbonate. *Geochim. Cosmochim. Acta*, **59,** 2265–2278.

Schulze, F., Lewy, Z., Kuss, J. and **Gharaibeh, A.** (2003) Cenomanian–Turonian carbonate platform deposits in west central Jordan. *Int. J. Earth Sci. (Geol. Rundsch.)*, **92,** 641–660.

Schulze, F., Marzouk, A.M., Bassiouni, M.A.A. and **Kuss, J.** (2004) The late Albian–Turonian carbonate platform succession of west-central Jordan: stratigraphy and crisis. *Cretaceous Res.*, **25,** 709–737.

Schulze, F., Kuss, J. and **Marzouk, A.** (2005) Platform configuration, microfacies and cyclicities of the upper Albian to Turonian of west-central Jordan. *Facies*, **50,** 505–527.

Shafik, S. (1990) Late Cretaceous nannofossil biostratigraphy and biogeography of the Australian western margin. *Australian Bureau of Mineral Resources, Geology and Geophysics, Report* 295, 164 pp.

Sinton, C.W., Duncan, R.A., Storey, M., Lewis, J. and **Estrada, J.J.** (1998) An oceanic flood basalt province within the Caribbean Plate. *Earth Planet. Sci. Lett.*, **155,** 221–235.

Sissingh, W. (1977) Biostratigraphy of Cretaceous calcareous nannoplankton. *Geol. Mijnbouw*, **56,** 37–65.

Skelton, P.W., Spicer, R.A., Kelley, S.P. and **Gilmour, I.** (2003) The Cretaceous World. Cambridge University Press, The Open University, Cambridge, 360 pp.

Sliter, W.V. (1968) Upper Cretaceous foraminifera from southern California and northwestern Baja California, Mexico. *Univ. Kansas Paleontol. Contrib.*, **49,** 1–141.

Snow, L.J., Duncan, R.A. and **Bralower, T.J.** (2005) Trace element abundances in the Rock Canyon Anticline, Pueblo, Colorado, marine sedimentary section and their relationship to Caribbean plateau construction and oxygen anoxic event 2. *Paleoceanography*, **20,** PA3005. DOI: 10.1029/2004PA001093.

Tantawy, A. (2003) Calcareous nannofossil biostratigraphy and paleoecology of the Cretaceous–Tertiary transition in the central Eastern Desert of Egypt. *Mar. Micropaleontol.*, **47,** 323–356.

Tantawy, A.A. (2008) Calcareous Nannofossil Biostratigraphy and Paleoecology of the Cenomanian–Turonian Transition at Tazra, Tarfaya Basin, southern Morocco. *Cretaceous Res.*, **29,** 995–1007.

Thiry, M. (2000) Palaeoclimatic interpretation of clay minerals in marine deposits: an outlook from the continental origin. *Earth-Sci. Rev.*, **49,** 201–221.

Trappe, J. (1992) Microfacies zonation and spatial evolution of a carbonate ramp: marginal Moroccan phosphate sea during the Paleogene. *Geol. Rundsch.*, **81,** 105–126.

Tsikos, H., Jenkyns, H.C., Walsworth-Bell, B., Petrizzo, M.R., Forster, A., Kolonic, S., Erba, E., Premoli Silva, I., Baas, M., Wagner, T. and **Sinningh Damste, J.S.** (2004) Carbon-isotope stratigraphy recorded by the Cenomanian–Turonian oceanic anoxic event: correlation and implications based on three key localities. *J. Geol. Soc.*, **161,** 711–719.

Turgeon, S.C. and **Creaser, R.A.** (2008) Cretaceous oceanic anoxic event 2 triggered by a massive magmatic episode. *Nature*, **454,** 323–326.

Uličný, D., Hladikova, J. and **Hradecka, L.** (1993) Record of sea-level changes, oxygen depletion and the delta-C-13 anomaly across the Cenomanian–Turonian boundary, Bohemian Cretaceous Basin. *Cretaceous Res.*, **14,** 211–234.

Van Buchem, F.S.P., Razin, P., Homewood, P.W., Heiko Oterdom, W. and **Philip, J.** (2002) Stratigraphic organization of carbonate ramps and organic-rich intraself: Natih Formation (middle Cretaceous) of northern Oman. *AAPG*, **86,** 1.

Voigt, S., Gale, A.S. and **Floegel, S.** (2004) Midlatitude shelf seas in the Cenomanian–Turonian greenhouse world: temperature evolution and North Atlantic circulation. *Paleoceanography*, **19,** PA4020. DOI: 10.1029/2004PA001015.

Voigt, A., Gale, A.S. and **Voigt, T.** (2006) Sea-level change, carbon cycling and palaeoclimate during the Late Cenomanian of northwest Europe: an integrated palaeoenvironmental analysis. *Cretaceous Res.*, **27,** 836–858. DOI: 10.1016/j.cretres.2006.04.005.

Wagner, T., Sinninghe Damste, J., Hofmann, P. and **Beckmann, B.** (2004) Euxinia and primary production in Late Cretaceous eastern equatorial Atlantic surface waters fostered orbitally driven formations of marine black shales. *Paleoceanography*, **19**. DOI: 10.1029/2003PA000898. Article no. PA3099.

Watkins, D.K., Wise, S.W., Pospichal, J.J. and **Crux, J.** (1996) Upper Cretaceous calcareous nannofossil biostratigraphy and paleoceanography of the Southern Ocean. In: *Microfossils and Oceanic Environments* (Eds A. Moguilevsky and R. Whatley), pp. 355–381. University of Wales, Aberystwyth Press, Aberystwyth.

Wiedmann, J., Butt, A. and **Einsele, G.** (1978) Vergleich von marokkanischen Kreide–Kusteaufschlussen und Tiefseebohrungen (DSDP): stratigraphie, palaoenvironment und subsidenz and einem passiven kontinentalrand. *Geol. Rundsch.*, **67,** 454–608.

Wiedmann, J., Butt, A. and **Einsele, G.** (1982) Cretaceous stratigraphy, environment, and subsidence history at the Moroccan continental margin. In: *Geology of the Northwest African Continental Margin* (Eds U. von Rad, K. Hinz, M. Sartheim and E. Seibold), pp. 366–395. Springer, Berlin.

Wignall, P.B. (2001) Large igneous provinces and mass extinctions. *Earth-Sci. Rev.*, **53,** 1–33.

Wilmsen, M. (2003) Sequence stratigraphy and palaeoceanography of the Cenomanian Stage in northern Geremany. *Cretaceous Res.*, **24,** 525–568.

Manuscript received 15 May 2009; revision accepted 27 January 2010